

Single-particle digitization strategy for quantum computation of a ϕ^4 scalar field theoryJoão Barata^{*}*Instituto Galego de Física de Altas Enerxías (IGFAE), Universidade de Santiago de Compostela, Santiago de Compostela, E-15782 Galicia, Spain*Niklas Mueller[†]*Department of Physics, University of Maryland, College Park, Maryland 20742, USA*Andrey Tarasov[‡]*Department of Physics, The Ohio State University, Columbus, Ohio 43210, USA
and Joint BNL-SBU Center for Frontiers in Nuclear Science (CFNS) at Stony Brook University, Stony Brook, New York 11794, USA*Raju Venugopalan[§]*Physics Department, Brookhaven National Laboratory, Bldg. 510A, Upton, New York 11973, USA*

(Received 21 December 2020; revised 11 March 2021; accepted 23 March 2021; published 8 April 2021)

Motivated by the parton picture of high-energy quantum chromodynamics, we develop a single-particle digitization strategy for the efficient quantum simulation of relativistic scattering processes in a $d + 1$ -dimensional scalar ϕ^4 field theory. We work out quantum algorithms for initial state preparation, time evolution, and final state measurements. We outline a nonperturbative renormalization strategy in this single-particle framework.

DOI: [10.1103/PhysRevA.103.042410](https://doi.org/10.1103/PhysRevA.103.042410)**I. INTRODUCTION**

Significant effort has been invested towards studying problems in quantum chemistry [1–4], condensed matter physics [5–7], cosmology [8–10], and in high-energy and nuclear physics [11–16], with digital quantum computers and analog quantum simulators [17–22]. A major motivation is to deepen our understanding of conventionally intractable features of the ground-state properties of strongly correlated many-body systems such as the spectrum of bound states. Another is to advance the state of the art in scattering problems, which provide dynamical information on such complex systems.

In this work, our focus will be on the problem of developing quantum algorithms for high-energy scattering and multiparticle production in relativistic quantum field theory. Underlying our work is the promising yet distant goal of extracting dynamical information on the properties of hadrons and nuclei in quantum chromodynamics (QCD).

Examples of scattering problems in QCD where quantum information science can accelerate our present computational capabilities are low-energy scattering in nuclear many-body systems [23,24], the thermalization process in ultrarelativistic ion-ion collisions [25], studies of the structure of nuclear matter probed in deeply inelastic scattering (DIS) of electrons off protons and nuclei [26–33], and the fragmentation of

quarks and gluons into jets of hadrons [34,35]. For instance, both jet fragmentation functions and DIS structure functions require one to compute autocorrelation functions of currents in Minkowski spacetime; this poses a challenge to classical Monte Carlo methods that are constructed to compute Euclidean spacetime correlators [36–43].

Quantum devices have the potential to overcome the limitations of classical computers in addressing many of the above problems. However, presently their limitation is that scattering problems involve a vast range of spatial (momentum) and temporal (energy) scales and require that a large number of (local) quantum field operators be quantum simulated. This is challenging with present day NISQ era technology restricted to few tens of non-error-corrected qubits [22].

As discussed in seminal papers by Jordan, Lee, and Preskill [44,45], quantum simulating scattering problems in relativistic quantum field theories requires a lattice discretization and, in the case of a bosonic theory, the truncation of the local Hilbert space of field operators. One can view such a digitization as defining a low-energy effective theory, in the sense of a generalized renormalization group (RG) [46]. We will argue here that, from this viewpoint, a digitization scheme does not necessarily need to be based on a decomposition of local field operators but, more generally, should be based on the most economical implementation of the relevant directions of the RG for a specific problem.

Pursuant to this goal, we will explore a digitization strategy for the bosonic field theory of a real scalar field in $d + 1$ spacetime dimensions based on a generalization of relativistic Bose-symmetrized “single-particle states” previously discussed by us in [31]. For a wide class of problems,

^{*}joaolourenco.henriques@usc.es[†]niklasmu@umd.edu[‡]tarasov.3@osu.edu[§]raju@bnl.gov

this digitization requires resources that are only logarithmic in volume \mathcal{V} (but linear in particle number), as opposed to field-operator-based approaches that depend linearly on the volume. We will discuss a strategy for initial state preparation, time evolution, and measurement for scattering processes in high-energy physics. Our time evolution algorithm has a gate complexity similar to that of [44,45]; however, because the basis states are eigenstates of the free Hamiltonian and of the particle number operator, initial state preparation and measurement are particularly simple.

Our approach is unusual in the sense that relativistic many-body systems are usually described by field operators within quantum field theory. In relativistic theories, particle number is not conserved and relativistic single-particle states in position space are not Fourier conjugates of single-particle states in momentum space. While it seems that these properties render quantum simulation of relativistic quantum field theory fundamentally different to those in quantum chemistry [1–4] or in nonrelativistic low-energy nuclear physics [11–13,23], we will demonstrate here that this is not the case and that we are able to utilize algorithms that are conceptually similar.

A powerful motivation underlying our approach is the single-particle picture [47] behind the well-known Feynman diagram techniques to compute scattering cross sections in high-energy physics at weak coupling. Because the computational complexity of Feynman diagram computations grows factorially with the required precision, their computation presents another opportunity for a quantum advantage [44,45]. Since, as noted, scattering problems can be formulated in terms of Minkowski space field correlators, a first principles path integral computation with classical Monte Carlo techniques is challenging. Albeit considering a simpler theory, our ultimate aim is to apply this approach to quantum simulate scattering problems in quantum chromodynamics; a first step towards this goal would be a hybrid strategy combining a quantum treatment of some of the scattering degrees of freedom with a classical treatment of the rest [31]. A relevant analogy in this regard is the simulation of quantum impurities in strongly correlated condensed matter systems [48], or the simulation of open quantum systems in heavy-ion collisions [49]. In light of the many challenges of NISQ era computing, the digitization strategy we will present may therefore offer a useful compromise between being able to make progress in a limited class of problems in high-energy physics with restricted resources and conceptual simplicity versus simulating any possible problem in quantum field theory in full generality.

This paper is organized as follows: In Sec. II we will discuss the conceptual basis of our approach to quantum computing scattering cross sections in high-energy physics. Our digitization strategy is discussed in Sec. III. In Sec. IV we will present the single-particle digitization algorithm for quantum computing scattering cross sections: state preparation is discussed in Sec. IV A, the implementation of the time evolution operator as a quantum circuit in Sec. IV B, the strategy to extract cross sections through measurements in Sec. IV C, and renormalization aspects of the problem in Sec. IV D. In Sec. V we summarize our results and discuss extensions of this approach to include theories with fermion and gauge fields with internal symmetries.

We elaborate on several of the discussions in the main text in multiple Appendixes. In Appendix A we provide details of the single-particle digitization strategy. In Appendix B we discuss the state preparation algorithm in greater detail. Appendixes C, D, and E contain details of the algorithm for the time evolution operator. Finally in Appendix F we provide further details of the renormalization procedure.

II. HIGH-ENERGY SCATTERING

Understanding the structure of matter at the subnucleon scales of nuclear and particle physics requires a wide range of scattering experiments. The theoretical foundations of these scattering problems is well developed within the framework of relativistic quantum field theory. The simplest formulation of a scattering process is through the S -matrix,

$$S_{\beta\alpha} \equiv \langle \Psi_{\beta}^{\text{out}} | \Psi_{\alpha}^{\text{in}} \rangle, \quad (1)$$

defined as the overlap of asymptotic in- ($|\Psi_{\alpha}^{\text{in}}\rangle$) and out- ($|\Psi_{\beta}^{\text{out}}\rangle$) states, which are time-independent eigenstates of the Hamiltonian $H = H_0 + V$.

In the Heisenberg picture, all nontrivial information on these states is encoded in the Lippmann-Schwinger equation [50,51],

$$|\Psi_{\alpha}^{\text{in/out}}\rangle = |\phi_{\alpha}\rangle + G_0 V |\Psi_{\alpha}^{\text{in/out}}\rangle = (V - V G_0 V)^{-1} V |\phi_{\alpha}\rangle,$$

where $|\phi_{\alpha}\rangle$ are single-particle eigenstates of the free Hamiltonian H_0 satisfying $H_0 |\phi_{\alpha}\rangle = E_{\alpha} |\phi_{\alpha}\rangle$, $G_0 \equiv (E_{\alpha} - H_0 \pm i\epsilon)^{-1}$ and $V - V G_0 V$ is the Schwinger operator. The S -matrix can also be expressed as

$$S_{\beta\alpha} = \delta_{\alpha\beta} - 2\pi i \delta(E_{\alpha} - E_{\beta}) T_{\beta\alpha}, \quad (2)$$

where energy conservation is explicit, and the T -matrix is defined as

$$T_{\beta\alpha} = \langle \phi_{\beta} | V | \Psi_{\alpha}^{\text{out}} \rangle = \langle \Psi_{\beta}^{\text{in}} | V | \phi_{\alpha} \rangle = \langle \Psi_{\beta}^{\text{in}} | (V - V G_0 V) | \Psi_{\alpha}^{\text{out}} \rangle. \quad (3)$$

The cross section for a scattering process $\alpha \rightarrow \beta$ is given by the modulus squared of $T_{\beta\alpha}$ (multiplied by kinematic factors),

$$|T_{\beta\alpha}|^2 = \langle \Psi_{\alpha}^{\text{in}} | (V - V G_0 V) P_{\beta}^{\text{out}} (V - V G_0 V)^{\dagger} | \Psi_{\alpha}^{\text{in}} \rangle, \quad (4)$$

with $P_{\beta}^{\text{out}} = |\Psi_{\beta}^{\text{out}}\rangle \langle \Psi_{\beta}^{\text{out}}|$. The T -matrix elements in Eq. (3) can be computed by solving the Lippmann-Schwinger equation. This can be achieved using analytic perturbative techniques such as the Born expansion [51] or nonperturbatively using Schwinger's variational principle [50], the Schwinger-Lanczos [52], or R -matrix approaches [53].

Quantum variants of these methods are currently under development; for an implementation of the Quantum-Lanczos algorithm in a scattering problem; see [54]. We will proceed here with the formulation of the quantum scattering problem in the time-dependent Schrödinger picture [45,55].

Before we proceed in that direction, we note that our single-particle digitization strategy for the S -matrix can be mapped on to a virial expansion, which is a “cluster” expansion in powers of the density that captures the many-body properties of a system at low particle densities. It is particularly successful in reproducing their ground-state

properties,¹ which are expressed as a density expansion in the n th-order virial coefficients²

$$b_n \propto \left[S^\dagger \frac{\partial S}{\partial E} \right]_n, \quad (5)$$

where $[S^\dagger \frac{\partial S}{\partial E}]_n$ of $n \rightarrow n$ scattering particles. Thus because our single-particle strategy is optimal for capturing the many-body dynamics of a relativistic theory at low occupancies, a computation of $n \rightarrow n$ scattering matrix elements will allow us to determine ground-state properties in our framework with the same range of validity as the virial expansion. Indeed, one can in principle go further and test the validity of this expansion relative to a direct computation of ground-state properties of relativistic many-body systems in our framework.

A. Schrödinger picture of S -matrix scattering

In the Schrödinger picture, the scattering process is described in terms of time-dependent wave packets

$$|\Psi_g^{\text{in/out}}(t)\rangle \equiv \int d\alpha g(\alpha) e^{-iE_\alpha t} |\Psi_\alpha^{\text{in/out}}\rangle, \quad (6)$$

where $g(\alpha)$ is a function that describes the localization of the wave packet. In this approach, the Lippmann-Schwinger equation can be expressed as

$$|\Psi_g^{\text{in/out}}(t)\rangle = |\phi_g(t)\rangle + \int_0^\infty dT e^{\pm i(H_0 \mp i\epsilon)T} V |\Psi_g^{\text{in/out}}(t \mp T)\rangle, \quad (7)$$

where $|\phi_g(t)\rangle$ is defined identically as in Eq. (6). The in-wave packet satisfies the boundary condition $|\Psi_g^{\text{in}}(-\infty)\rangle = |\phi_g(-\infty)\rangle$ at negative infinity, and the out-wave packet satisfies a similar condition at positive infinity. In the Schrödinger picture, one may interpret $V(T) \equiv V e^{-\epsilon|T|}$ as adiabatically turning on the interaction to obtain $|\Psi^{\text{in}}(t)\rangle$ from evolution of the initial condition $|\phi_g(-\infty)\rangle$ using Eq. (7) and likewise, in reverse, for $|\Psi_g^{\text{out}}\rangle$. This approach, employing single-particle wave packets, will form the basis of our algorithm in Sec. IV.

B. Spacetime picture of scattering experiments at high energies

At high energies, the gap of single-particle states to continuum particle-antiparticle pairs becomes small, and a description of scattering in terms of the second quantized language of quantum field operators appears natural. Quantum simulation of this problem is desirable because of the well-known challenges of classical computation.

However, interestingly, at high energies, for a wide class of scattering problems, single-particle digitization strategies applied at lower energies may be viable and indeed desirable. The latter can be understood straightforwardly in the context

of the scattering of two protons at the ultrarelativistic energies of the Large Hadron Collider (LHC). The wave packets of the two colliding protons can be constructed formally, along the lines of Eq. (6); however, such wave packets, as observed by Bjorken and Feynman, for many final states of interest in scattering at high energies are accurately described in terms of the scattering of pointlike “parton” (quark, antiquark, and gluon) constituents within the protons that are eigenstates of the free QCD Hamiltonian [28,62]. In this parton picture of high-energy scattering, as we will now discuss, the switch-on and off time τ_0 and the interaction time τ_I can be related to physical timescales.

These timescales are best understood in the context³ of the deeply inelastic scattering (DIS) of electrons (and other leptons) off protons and nuclei. In DIS, the incoming electron emits a virtual photon that strikes a quark or antiquark within the hadron, thereby providing information on the quark and (indirectly) gluon distributions within. The relevant DIS kinematic variables are the momentum resolution Q of the probe (with $Q^2 \gg \Lambda_{\text{QCD}}^2$, the QCD confinement scale) and the Bjorken variable $x_{\text{Bj}} \approx Q^2/s$, where \sqrt{s} is the DIS center-of-mass energy.

In the QCD parton model, $x_{\text{Bj}} \sim x$ is the momentum fraction of the hadron carried by the struck quark or antiquark. The DIS cross section at large x_{Bj} corresponds to the projection of the hadron wave function into a Fock state that is a direct product state of single-particle parton states that make up the hadron’s quantum numbers. In contrast, the small x_{Bj} (high-energy) cross section corresponds to the scattering of the virtual photon off a Fock state containing a large number of partons, most of which carry a small fraction ($x \ll 1$) of the hadron’s momentum.

The physically motivated time required to probe fluctuations of the proton into differing parton configurations is the Ioffe time [63] $\tau_0 \sim \tau_{\text{Ioffe}} = 1/(2M_p x_{\text{Bj}})$, with M_p the proton mass; in the DIS example, this gives the coherence time of the fluctuation of the virtual photon into a parton state in the rest frame of the proton or nuclear target.⁴ Likewise in DIS, the interaction time of the probe is the typically much shorter timescale $\tau_I \sim 1/Q$. A minimal bound on this timescale is τ_W , the Wigner time delay defined as $\partial S/\partial E$, where E denotes energy, in the virial expansion, we discussed previously, of a scattering process of $n \rightarrow m$ particles [56–61,65].⁵

The parton picture is manifest when field theories are quantized [71] on a lightlike surface $x^+ = 0$, with the light-cone Hamiltonian $P^- = P_0^- + V$, defined as the generator

³We refer readers unfamiliar with DIS to our paper [31] for some of the key references and for a discussion of aspects of this scattering problem from a quantum computing perspective.

⁴In general, the coherence time is a distribution, with the stated value being the upper bound. For fluctuations of the virtual photon into a highly excited QCD Fock state, coherence time estimates are considerably shorter [64].

⁵The generalization of these ideas relating asymptotic scattering phase shifts to differences in energy levels of static quantities in a finite box was pioneered by Luscher [66,67]. It is an active area of research in lattice gauge theory [68,69], recently discussed in the context of quantum computing [70].

¹The extension of the virial expansion to nonequilibrium autocorrelation functions is highly nontrivial; an excellent review of this topic can be found in [56,57].

²This expression, originally formulated as a quantum many-body extension [58,59] to the famous Beth-Uhlenbeck formula was later generalized to discuss relativistic many-body $n \leftrightarrow m$ inelastic processes [60,61].

of translations in x^+ . The Galilean subgroup of the lightfront Poincaré group is isomorphic to the symmetry group of two-dimensional quantum mechanics [72], allowing one to formulate scattering problems in quantum field theory in the language of nonrelativistic quantum mechanics. In particular, due to time dilation at high energies, the lightfront potential is suppressed (by powers of the energy) relative to the kinetic term; Fock states, which are single-particle direct product states of partons, therefore provide a good eigenbasis for high-energy scattering [73].

Even though the single-particle picture of high-energy scattering finds an elegant representation in lightfront quantization, it is not restricted to it. It is a generic feature of Feynman diagrams in perturbation theory [74] and more recently of so-called “conformal truncation” methods [75–77] introduced in the context of conformal field theory [78]. This property of high-energy scattering motivates exploring a single-particle digitization strategy, which we will discuss at length in the rest of this paper in conventional equal time quantization.⁶ Further, as detailed in Sec. IV C, this approach is particularly valuable in performing measurements on a quantum computer.

Our single-particle digitization strategy will encounter significant challenges when applied to gauge theories. Concretely, when applied to the digitization of theories coupled to gauge fields, the presented time evolution strategy must be modified, as we discuss further in Sec. V. Nevertheless one may be able to make progress employing this strategy in physical problems where hybrid quantum and classical techniques are applicable; in QCD, these include these include effective field theories (EFTs) for jet physics [81], high parton densities (small x) [82] and at finite temperature [83], and a lattice EFT for computing parton distributions [38].

III. SINGLE-PARTICLE STRATEGY

In this section, and in the next, we will develop a single-particle digitization strategy for a relativistic (real) scalar field theory with local quartic interactions in $d + 1$ spacetime dimensions. The Hamiltonian for this theory is given by

$$\bar{H} = \int d^d \mathbf{x} \left[\frac{\pi_{\mathbf{x}}^2}{2} + \frac{1}{2} (\nabla \phi_{\mathbf{x}})^2 + \frac{\bar{m}^2}{2} \phi_{\mathbf{x}}^2 + \frac{\bar{\lambda}}{4!} \phi_{\mathbf{x}}^4 \right], \quad (8)$$

where \bar{m} and $\bar{\lambda}$ are the (bare) mass and quartic coupling, and ∇ is the spatial gradient operator in d dimensions. The Heisenberg field operators are

$$\phi_{\mathbf{x}} = \int \frac{d^d \mathbf{p}}{(2\pi)^d} \frac{1}{\sqrt{2\bar{\omega}_{\mathbf{p}}}} [a_{\mathbf{p}} + a_{-\mathbf{p}}^\dagger] e^{i\mathbf{p}\cdot\mathbf{x}}, \quad (9)$$

which satisfies, with its canonical conjugate operator $\pi_{\mathbf{x}}$, the equal-time commutation relations $[\phi_{\mathbf{x}}, \pi_{\mathbf{y}}] = i\delta^{(d)}(\mathbf{x} - \mathbf{y})$. The annihilation (creation) operators $a_{\mathbf{p}} (a_{\mathbf{p}}^\dagger)$ are momentum-space Fock operators, corresponding to a set of harmonic oscillators with frequency $\bar{\omega}_{\mathbf{p}} = \sqrt{\mathbf{p}^2 + \bar{m}^2}$ and commutation

relations $[a_{\mathbf{p}}, a_{\mathbf{k}}^\dagger] = (2\pi)^d \delta^{(d)}(\mathbf{p} - \mathbf{k})$, $[a_{\mathbf{p}}, a_{\mathbf{k}}] = [a_{\mathbf{p}}^\dagger, a_{\mathbf{k}}^\dagger] = 0$. Single-particle states are defined as

$$|\mathbf{p}\rangle^{\text{phys}} \equiv \sqrt{2\bar{\omega}_{\mathbf{p}}} a_{\mathbf{p}}^\dagger |\text{vac}\rangle, \quad (10)$$

which satisfy the relativistic normalization condition $\langle \mathbf{p} | \mathbf{k} \rangle^{\text{phys}} = 2\bar{\omega}_{\mathbf{p}} \delta^{(3)}(\mathbf{p} - \mathbf{k})$, where $|\text{vac}\rangle$ denotes the Fock vacuum.

We discretize the theory on a spatial lattice of size N_s^d and express the Hamiltonian (in dimensionless units) as

$$H \equiv a_s \bar{H} = \sum_{\mathbf{n}} \left[\frac{1}{2} \pi_{\mathbf{n}}^2 + \frac{1}{2} (\nabla \phi_{\mathbf{n}})^2 + \frac{m^2}{2} \phi_{\mathbf{n}}^2 + \frac{\lambda}{4!} \phi_{\mathbf{n}}^4 \right], \quad (11)$$

where $m = \bar{m} a_s$, $\lambda = \bar{\lambda} a_s^{4-d}$ are dimensionless bare mass and coupling parameters, a_s the lattice spacing, and $\mathbf{n} = (n_1, \dots, n_d)$, $n_i \in [0, N_s - 1]$ labels a point $\mathbf{x} = \mathbf{n} a_s$ on the lattice. We will likewise define a momentum space lattice vector $\mathbf{q} = (q_1, \dots, q_d)$, $q_i \in [-\frac{N_s}{2}, \frac{N_s}{2} - 1]$. The lattice field operators are

$$\begin{aligned} \phi_{\mathbf{n}} &= \frac{1}{\sqrt{\mathcal{V}}} \sum_{\mathbf{q}} \frac{1}{\sqrt{2\omega_{\mathbf{q}}}} [a_{\mathbf{q}} + a_{-\mathbf{q}}^\dagger] e^{i2\pi\mathbf{n}\cdot\mathbf{q}/N_s}, \\ \pi_{\mathbf{n}} &= \frac{-i}{\sqrt{\mathcal{V}}} \sum_{\mathbf{q}} \sqrt{\frac{\omega_{\mathbf{q}}}{2}} [a_{\mathbf{q}} - a_{-\mathbf{q}}^\dagger] e^{i2\pi\mathbf{n}\cdot\mathbf{q}/N_s}, \end{aligned} \quad (12)$$

where $\mathcal{V} = N_s^d$ and $\omega_{\mathbf{q}} = \bar{\omega}_{\mathbf{q}} a_s^{-1}$ is the dimensionless energy. Note that we use the same notation for the dimensionless lattice Fock operators $a_{\mathbf{q}}$ and the dimensionful continuum operators in Eq. (9).

We will implement below the time evolution operator of the free Hamiltonian [setting $\lambda = 0$ in Eq. (11)] in the momentum representation. This allows us to use the continuum dispersion relation $\omega_{\mathbf{q}} = \sqrt{\mathbf{p}^2 + m^2}$ [$\mathbf{p} \equiv \mathbf{p}(\mathbf{q})$], as opposed to the lattice dispersion relation that one has when working in position space; this potentially reduces discretization errors significantly.

The key idea in our digitization scheme is to decompose the many-particle Hilbert space into single-particle sectors $\mathcal{H} = \bigotimes_{l=0}^{\infty} \mathcal{H}^l$, where a number of qubits are used to represent either momentum or position eigenstates in a binary decomposition. Since we are dealing with a relativistic theory where particle number is not conserved, an additional qubit is used to indicate whether or not a particle “exists.” With this in mind, the single-particle Hilbert space is spanned by

$$\mathcal{H}^l = \text{span}\{|\Omega\rangle^{(l)}, \{|\mathbf{q}\rangle^{(l)}\}\}, \quad (13)$$

where Ω denotes “empty states, and $|\mathbf{q}\rangle$ “occupied states. Further, a “register” of $N \equiv \log_2 \mathcal{V} + 1$ spins (qubits) represents a relativistic single-particle state with momentum $\mathbf{q} = (\mathbf{q}_1, \dots, \mathbf{q}_d)$ in d dimensions,

$$|\mathbf{q}\rangle^{(l)} \equiv |\mathbf{q}_1, \dots, \mathbf{q}_d\rangle |\uparrow\rangle, \quad (14)$$

where one qubit $|\mathbf{n}\rangle = |\uparrow\rangle$ denotes that the single-particle state is occupied. Each momentum component of the occupied single-particle state

$$|q_i\rangle \equiv |s_i\rangle | |q_i| \rangle \quad (15)$$

is represented by $(N - 1)/d$ qubits, where $s_i = \text{sign}(q_i)$ is the sign (one qubit) and $|q_i|$ the absolute value (abs). Likewise, we

⁶For recent work on quantum computing in lightcone quantization, see [79,80].

define an unoccupied single-particle state as a state where abs, sign, and occupation number qubits are all in the $|\downarrow\rangle$ state,

$$|\Omega\rangle^{(l)} \equiv |\downarrow^{\otimes d \cdot N^{\text{abs}}}, \downarrow^{\otimes d}, \downarrow\rangle, \quad (16)$$

and the Fock vacuum is defined as $|\text{vac}\rangle = \bigotimes_l |\Omega\rangle^{(l)}$. We will represent these momentum states using a binary encoding with the qubits representing the digits. In this case, $N^{\text{abs}} = \frac{N-1}{d} - 1 = \frac{\log_2(\mathcal{V}/2^d)}{d}$ qubits.⁷ States with zero occupation number but finite \mathbf{q} are unphysical and are excluded. Concrete examples of this single-particle digitization scheme are given in Appendix A. The normalization $\langle \mathbf{q} | \mathbf{q}' \rangle = \delta_{\mathbf{q}, \mathbf{q}'}$ of these basis states differs from the relativistic normalization in Eq. (10), with $|\mathbf{q}\rangle = |\mathbf{p}\rangle^{\text{phys}} / \sqrt{2\omega_{\mathbf{q}}}$. A generic state $|\psi\rangle^{(l)} \in \mathcal{H}^l$ can be written as

$$|\psi\rangle^{(l)} = a_0 |\Omega\rangle^{(l)} + \sum_{\mathbf{q}} a_{\mathbf{q}} |\mathbf{q}\rangle^{(l)}, \quad (17)$$

with $|a_0|^2 + \sum_{\mathbf{q}} |a_{\mathbf{q}}|^2 = 1$. The free part of the Hamiltonian (H_0) is block diagonal with the blocks labeled by the number of particles. Particle number eigenstates are on-shell single-particle states and those that do not correspond to virtual particles.

The Fock operators in Eq. (12) for the M many-particle states on the combined Hilbert space $\mathcal{H} = \bigotimes_{l=0}^{\infty} \mathcal{H}^l$ are

$$a_{\mathbf{q}} \equiv \lim_{M \rightarrow \infty} \frac{1}{\sqrt{M}} \sum_{l=0}^{M-1} a_{\mathbf{q}}^{(l)}, \quad (18)$$

with $a_{\mathbf{q}}^{(l)}, a_{\mathbf{q}}^{(l)\dagger}$ denoting chains of spin raising and lowering operators for each \mathbf{q} , and $(a_{\mathbf{q}}^{(l)\dagger})^2 = (a_{\mathbf{q}}^{(l)})^2 = 0$. In practice, one truncates the number of single-particle registers at a finite M . If M is large compared to the typical occupancy of a state $\mathbf{n} \equiv \sum_i \mathbf{n}^{(i)}$, the bosonic commutation algebra is realized, $[a_{\mathbf{q}}, a_{\mathbf{q}'}^\dagger] = \delta_{\mathbf{q}, \mathbf{q}'} + O(\frac{\mathbf{n}}{M})$. Additional details of the construction are presented in Appendix A.

In the single-particle digitization of the Hilbert space of the scalar field theory, its dimension grows logarithmically with the volume \mathcal{V} and linearly with M . This is ideal for high-energy scattering problems, where the particle number density is small, such as the Bjorken limit [26–29] of the DIS problem we discussed earlier. The digitization is not economical for a very dense system because, as we will discuss, Bose symmetrization creates a large overhead of unphysical states. However, as we also noted, our digitization strategy could potentially be extended to such dense systems employing a hybrid quantum and classical approach.

IV. QUANTUM ALGORITHM

In this section, the single-particle digitization strategy will be formulated as a concrete algorithm to quantum compute scattering cross sections. In line with the spacetime picture discussed in Sec. II, and paralleling the approach of Jordan,

⁷To avoid a sign ambiguity, we choose the lattice such that $q_i = 0$ is excluded. Then $s_i = \uparrow(\downarrow)$ is a positive (negative) sign. We use a physical convention $|\uparrow/\downarrow\rangle$ of up and down spins to label states, instead of the more common $|0/1\rangle$ notation.

Lee, and Preskill [45,55], the components of our algorithm are

- (A) Initial state preparation, discussed in Sec. IV A.
- (B) Simulating the time evolution, discussed in Sec. IV B.
- (C) Measurement of observables and their relation to scattering cross sections, discussed in Sec. IV C.
- (D) Renormalization, discussed in Sec. IV D.

These different elements are compactly summarized in Fig. 1.

We will first discuss the preparation of the initial state of noninteracting particles in spatially separated wave packets. Their preparation is particularly simple using the digitization presented in Sec. III compared to the field-based approach of [45,55,84], because single-particle states and the vacuum are computational basis states. Our algorithm consists of preparing a quantum mechanical superposition of these basis states to form wave packets, placing them in separated regions of phase space and finally Bose symmetrization of the resulting few or many-body wave function.

To implement the time evolution operator, we will employ a Suzuki-Trotter scheme⁸ [87,88]. We will treat the time evolution of the free and interacting parts of the Hamiltonian in Eq. (11) separately. We first evolve the wave packet with the free Hamiltonian H_0 , which is diagonal in the momentum representation. This is followed by a squeezing operation (analogous to that performed in quantum optics [89,90]), a quantum Fourier transformation [91] from momentum space to position space, and an implementation of the interaction term in position space, where it is local.

This algorithm differs from the field-based approach of [45,55,84] where the time evolution operator is split into a part diagonal in the $\phi_{\mathbf{x}}$ -basis and one diagonal in the conjugate $\pi_{\mathbf{x}}$ -basis. While the overall Trotter complexity scales as $O(\mathcal{V})$ in both cases, an important difference is that we avoid the lattice discretization of the Laplacian in Eq. (11) by working directly in momentum space.

Time evolution involves a switch-on of interactions from the noninteracting theory in the infinite past, $m(0) \equiv m_0$, $\lambda(0) = 0$ (in practice at some finite time $t = 0$) towards acquiring the renormalized, physical couplings $m(\tau_0) \equiv m^{\text{ren}}$, $\lambda(\tau_0) = \lambda^{\text{ren}}$ at $t = \tau_0$ right before the particles collide. The nonperturbative renormalization in the single-particle framework, which differs from that of [45,55], is discussed in Sec. IV D.

An important practical issue for the quantum algorithm is the spreading of the wave packets during the switch-on time of interactions, which may potentially cause the wave packets to interact before the coupling is turned to its final value. For this one may use the “forward-backward” evolution scheme outlined in [45,55]. Note, however, that because at large energies the dispersion is approximately linear $\omega \sim |\mathbf{p}|$,

⁸For practical applications, it is important to note that more efficient algorithms for time evolution exist. One such example is the linear combination of unitaries [85], later generalized to the method of quantum singular transformations [86]. The latter class of quantum algorithms not only significantly speeds up time evolution, but is also an efficient replacement of the classic phase estimation algorithm discussed in the context of measurements in Sec. IV C.

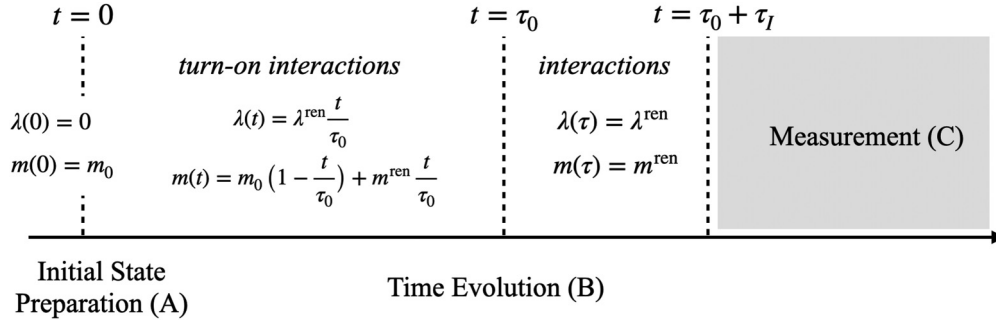


FIG. 1. Overview of the general algorithm to quantum compute high-energy scattering cross sections, including the values of the bare couplings λ and m for simulation time t . Initial state preparation is discussed in Sec. IV A, time evolution in Sec. IV B, and measurement of particle cross sections in Sec. IV C. The choice of (renormalized) couplings $\lambda(t)$, $m(t)$ is discussed in Sec. IV D.

the spreading of the wave packets is anticipated to be small [92].

Another relevant point is that the adiabatic preparation of single-particle states [45,55] will require a very large number of Trotter steps at high energies and likewise for the turn-off of interactions. This can be understood by considering the energy gap between single-particle states with momentum \mathbf{p} and energy $E = (\mathbf{p}^2 + m^2)^{\frac{1}{2}}$, and the lowest of the two-particle states with total momentum $\tilde{\mathbf{p}} \equiv \mathbf{p}_1 + \mathbf{p}_2$ (with relative momentum $\tilde{\mathbf{q}} \equiv \mathbf{p}_1 - \mathbf{p}_2 = 0$) and energy $E = [\tilde{\mathbf{p}}^2 + (2m)^2]^{\frac{1}{2}}$ at weak coupling. Because this gap vanishes as $\mathbf{p} \rightarrow \infty$ and $\tilde{\mathbf{p}} \rightarrow \infty$, adiabatic state preparation is all but impractical at high energies.

Different state preparation algorithms have been suggested [93–98] which are potentially faster than adiabatic state preparation. We note, however, that, departing from the strictly idealized S -matrix picture, in scattering processes such as DIS in QCD discussed in Sec. II B, the Ioffe time and like physical scales are the relevant timescales for state preparation and may allow for quicker nonadiabatic state preparation. Because the algorithm discussed below is general, and one may also make use of alternative state preparation algorithms [93–98], we will not say anything further beyond noting this interesting possibility.

We will discuss finally in this section the determination of scattering cross sections, utilizing a natural connection of our digitization strategy to particle physics concepts. In contrast to field-based digitizations [45,55], particle number measurements do not require any additional gate operations. Measurement of energy density or momentum, for example, via a phase estimation algorithm, have a simple gate complexity. Some of the “classical analysis” in high-energy experiments, of binning data or imposing kinematic cuts, can be incorporated directly in the quantum algorithm. We argue that, using novel techniques such as oblivious amplitude amplification [91,99,100], a quantum computer could possibly “beat” an actual particle physics experiment by producing rare events with a higher probability.

A. Initial state preparation

We will now discuss the state preparation of a Bose-symmetric state of single-particle wave packets at $t = 0$ and zero coupling that are well separated in position space. As a

first step, we create wave packets separately in n of the M particle registers (where n is the number of initial scatterers, typically $n = 2$). Each wave packet $i = 0, \dots, n - 1$ is centered at $(\bar{\mathbf{x}}_i, \bar{\mathbf{p}}_i)$ and is Gaussian distributed with a width $(\Delta\mathbf{x}, \Delta\mathbf{p})$ around this center, where $|\Delta\mathbf{x}| \ll |\bar{\mathbf{x}}_i - \bar{\mathbf{x}}_j|$ for all $i \neq j$ (here assumed to be identical for all particles). Typically one chooses $|\Delta\mathbf{x}| \sim 1/m$, and $|\mathbf{p}| \gg |\Delta\mathbf{p}| \sim m$, where m is the mass (in dimensionless units), so that particles are well localized on macroscopic scales.

Wave packets comprised of single-particle states $|\mathbf{q}\rangle$, located at the origin $(\bar{\mathbf{x}}_i, \bar{\mathbf{p}}_i) = (0, 0)$, are written⁹ in a momentum space representation as

$$|\Psi\rangle = \frac{1}{\sqrt{V}} \sum_{\mathbf{q}} \Psi_{\mathbf{q}} |\mathbf{q}\rangle, \quad (19)$$

where $\Psi_{\mathbf{q}}$ is a real, positive, and strongly localized distribution such as a Gaussian distribution. Each such wave packet can be translated to $(\bar{\mathbf{x}}_i, \bar{\mathbf{p}}_i) \neq (0, 0)$ such that as previously, $|\bar{\mathbf{x}}_i - \bar{\mathbf{x}}_j| \gg |\Delta\mathbf{x}|$, and $\bar{\mathbf{p}}_i$ corresponds to projectile kinematics, using circuits we will discuss shortly.

To create a wave packet in the momentum space representation, centered at $(\bar{\mathbf{x}}_i, \bar{\mathbf{p}}_i) = (0, 0)$, and with width $\Delta\mathbf{p}$ ($|\Delta\mathbf{x}| \sim |\Delta\mathbf{p}|^{-1}$), from the vacuum state $|\Omega\rangle$ [Eq. (16)] we use a simple variant of the algorithm in [101,102], which we illustrate below for $d = 1$ spatial dimensions. First, accounting for the $\mathbf{q} \rightarrow -\mathbf{q}$ symmetry of $\Psi_{\mathbf{q}}$, we first flip the occupation number qubit and then apply the Hadamard gate (H) to the sign qubit,

$$|\downarrow^{\otimes N^{\text{abs}}}, \downarrow, \downarrow\rangle \xrightarrow{\sigma^x, H} \frac{1}{\sqrt{2}} [|\downarrow^{\otimes N^{\text{abs}}}, \uparrow, \uparrow\rangle + |\downarrow^{\otimes N^{\text{abs}}}, \downarrow, \uparrow\rangle]. \quad (20)$$

Subsequently, we rotate all remaining $N^{\text{abs}} \sim \log_2(N_s)$ qubits by an angle $\theta_k = \pi/4 - \epsilon_k$,

$$|\downarrow\rangle^{(k)} \rightarrow \cos(\theta_k) |\downarrow\rangle^{(k)} + \sin(\theta_k) |\uparrow\rangle^{(k)}, \quad (21)$$

where $k \in [0, N^{\text{abs}} - 1]$ and $\epsilon_k \in [0, \pi/4]$. Thus for each $|\downarrow\rangle^{(k)}$ the state gets a $\cos(\theta_k)$ coefficient, while each $|\uparrow\rangle^{(k)}$

⁹We will henceforth drop the label (l) denoting a particular single-particle state, as in Eq. (17).

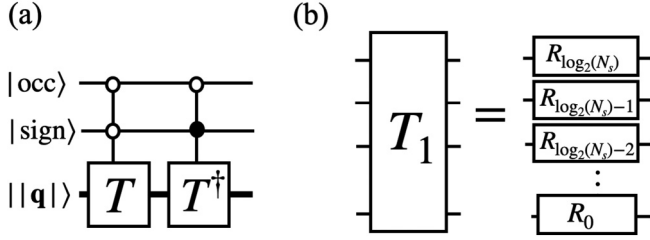


FIG. 2. (a) Translation operator for $d = 1$, where we abbreviate $T \equiv T_{n_1}^{(1)} = (T_1^{(1)})^{|n_1|}$ for $n_1 > 0$ and $(T_1^{(1)\dagger})^{|n_1|}$ for $n_1 < 0$. A white (black) circle indicates control by the $|\uparrow\rangle$ ($|\downarrow\rangle$) state. (b) For decomposition of the circuit, see text for details.

receives a $\sin(\theta_k)$ contribution. One can relate each ϵ_k to a specific distribution.¹⁰

Subsequently, we displace the centers of every single-particle wave packet in position and momentum space, such that they are widely separated $|\bar{\mathbf{x}}_i - \bar{\mathbf{x}}_j| \gg |\Delta\mathbf{x}|$, with $\bar{\mathbf{p}}_i$ denoting the initial momentum of each projectile. To achieve this, we need to use the translation operator $T_{\mathbf{n}}$ ($T_{\mathbf{q}}$) in position space (momentum space), defined as

$$T_{\mathbf{n}}|\mathbf{q}\rangle = e^{-i2\pi\mathbf{n}\cdot\mathbf{q}/N_s}|\mathbf{q}\rangle, \quad T_{\mathbf{n}}|\Omega\rangle = |\Omega\rangle, \quad (22)$$

where $\mathbf{x} = \mathbf{n}\mathbf{a}_s$ and $\mathbf{n} = (n_1, \dots, n_d)$. It can be decomposed in terms of one-dimensional translation operators $T_{\mathbf{n}} \equiv \bigotimes_{k=1}^d T_{n_k}^{(k)}$. To illustrate the circuit implementation of $T_{n_k}^{(k)}$, we will consider the operator for a translation by one lattice site in the positive direction $T_1^{(k)}$. A finite translation can then be achieved by successive applications of $T_{n_k}^{(k)} = (T_1^{(k)})^{n_k} (T_{n_k}^{(k)} = (T_1^{(k)\dagger})^{|n_k|})$ if $n_k > 0$ ($n_k < 0$), or directly via a simple modification of the algorithm for $T_1^{(k)}$, with identical gate complexity.

The circuit for an infinitesimal translation¹¹ T_1 is given in Fig. 2 acting on a state in the momentum space basis, using the gate $R_i \equiv \text{diag}(1, \exp\{-2\pi i/2^i\})$. Because the operators T and T^\dagger act on the register containing $|\mathbf{q}\rangle$, their action is controlled by the sign qubit to account for the sign in the exponent of Eq. (22). The momentum translation operator $T_{\mathbf{q}}$ can be implemented using exactly the same circuit, preceded by a change of basis $|\mathbf{q}\rangle \rightarrow |\mathbf{n}\rangle$ (via a quantum Fourier transform, as will be discussed in Sec. IV B 3). The generalization to arbitrary d is straightforward and has $O(M \log(\mathcal{V}))$ circuit complexity.¹²

The result of this procedure are multiparticle initial states comprising widely separated, nonoverlapping, wave packets $|\Psi_i\rangle$, and “empty” vacuum registers $|\Omega\rangle$,

$$|\phi\rangle \equiv |\Psi_0, \Psi_1, \dots, \Psi_{n-1}, \Omega, \dots, \Omega, \dots\rangle. \quad (23)$$

The corresponding Bose-symmetrized state is given by

$$|\phi_B\rangle \equiv \frac{1}{\sqrt{\mathcal{N}}} \sum_P \hat{P}|\phi\rangle, \quad (24)$$

¹⁰This distribution should be one that is probabilistic, namely, efficiently integrable with importance sampling techniques [101].

¹¹We will consider now the $d = 1$ case and drop the label k .

¹²Assuming large volumes, we will not discuss the action of the translation operator on the spatial boundaries.

where \hat{P} is the Bose permutation operator and $\mathcal{N} = M!/(M-n)!$.

To prepare $|\phi_B\rangle$ [Eq. (24)] from $|\phi\rangle$ [Eq. (23)], we will use a variant of an algorithm which, for the case $n = 1$, $M = 2$, we can illustrate as

$$\begin{aligned} |\Psi, \Omega\rangle|0\rangle &\xrightarrow{H} |\Psi, \Omega\rangle \frac{1}{\sqrt{2}}[|0\rangle + |1\rangle] \\ &\xrightarrow{\text{CSWAP}} \frac{1}{\sqrt{2}}[|\Psi, \Omega\rangle|0\rangle + |\Omega, \Psi\rangle|1\rangle] \\ &\xrightarrow{\text{CNOT}} \frac{1}{\sqrt{2}}[|\Psi, \Omega\rangle + |\Omega, \Psi\rangle]|0\rangle = |\phi_B\rangle. \end{aligned} \quad (25)$$

The basic idea is to introduce $s \equiv \log_2(M!/(M-n)!) \sim O(M^n)$ ancilla qubits ($s = 1$ in this example), which are prepared in a symmetric Bell superposition state. Each term in this superposition controls a specific SWAP operation between pairs of particle registers. The CNOT operation uses the occupation number qubits of the registers to uncompute the ancilla. Circuits for arbitrary n and M do not differ fundamentally from this example but are slightly more complicated and are discussed in Appendix B.

In particular, if M and n cannot be chosen such that s is an integer, one must choose $s = \lceil \log_2(M!/(M-n)!) \rceil \sim O(M^n)$, where the symbol $\lceil y \rceil$ denotes the smallest integer larger than y . As discussed in Appendix B, the symmetrization yields some unwanted permutations in this case which are eliminated through measurements and the symmetrization procedure becomes probabilistic as opposed to exact if $\log_2[M!/(M-n)!]$ is an integer. The chance of returning the desired state is $p_{\text{success}} = \mathcal{N}/2^s \geq 1/2$. As shown in Appendix B, one can always pick M for fixed n such that the probability of success is maximized. Note that the uncomputation of the s ancilla qubits for $n \geq 2$ requires using information stored in the momentum and position registers as control qubits. Fermionic states can be prepared along similar lines.¹³

Particles generated during the time evolution of the initial state are accommodated by a large number of empty registers $n_\Omega \equiv M - n \approx M \gg n$ initially. A rough estimate for M is the number of particles in the final state, ranging widely with energy from a few to few tens to few hundreds, an upper bound for which is the ratio of the collision energy to the particle mass \sqrt{s}/\bar{m} . This estimate does not include virtual states the system could be fluctuating into over shorter timescales. In weak coupling, there is a one-to-one correspondence between the Fock space explored in our digitization and that described by Feynman diagrams, allowing us to estimate that M should scale as the number of all internal and external lines. In the strong coupling limit, no such estimate is available, and thus explicit numerical analysis, including a nonperturbative renormalization procedure, will be required.

This algorithm for initial state preparation can be contrasted with the corresponding one in the field-based digitization [45,55]. In the latter case, one first prepares the noninteracting vacuum state in a Gaussian basis state using

¹³The authors plan to return to this case in future work, with the expectation that this leads to novel fermion-qubit mappings [103].

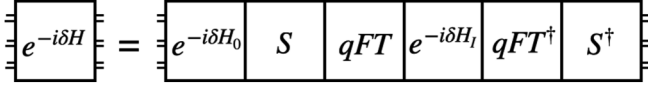


FIG. 3. Overview of the time evolution scheme for one Trotter-Suzuki step δ . Here S (discussed in Sec. IV B 2) and qFT (discussed in Sec. IV B 3) denote the squeezing operation and the quantum Fourier transformation, respectively.

the algorithm of [104], while in our case the vacuum is a computational basis state. Second, one employs a Suzuki-Trotter scheme to realize the application of position space Fock operators onto the vacuum state approximated by a linear combination of the field operators $\phi_{\mathbf{x}}$ and $\pi_{\mathbf{x}}$ in a region of space. In this case, Bose symmetrization is built into the realization of operators $\phi_{\mathbf{x}}$ and $\pi_{\mathbf{x}}$ and does not need to be enforced explicitly. In our case, a superselection rule specifies the physical sector removing unsymmetrized states.

B. Time evolution

We will follow a Trotter-Suzuki scheme with $N_\delta = (t - t_0)/\delta$ steps to implement the time evolution operator,

$$\begin{aligned} U(t, t_0) &\equiv e^{-iH(t-t_0)} = (e^{-iH\delta})^{N_\delta} + O(\delta^2) \\ &= (e^{-iH_I\delta} e^{-iH_0\delta})^{N_\delta} + O(\delta^2) \equiv (U_I U_0)^{N_\delta} + O(\delta^2), \end{aligned} \quad (26)$$

separating the evolution operator into free $U_0 \equiv \exp\{-iH_0\delta\}$ and interacting $U_I \equiv \exp\{-iH_I\delta\}$ parts, where H_0 is given by the quadratic terms and H_I by the ϕ^4 interaction term in Eq. (11).

We implement U_0 in the momentum space basis of Bose-symmetrized states (13)–(17), where it is diagonal. Using a combined squeezing operation and Fourier transformation, the interaction part U_I is then implemented in position space where it is local. Our strategy is summarized in Fig. 3, and the different elements are worked out below.

1. Free part U_0

The infinitesimal (normal-ordered) time evolution operator U_0 is given by

$$\begin{aligned} U_0 &\equiv \exp\left\{-i\delta \sum_{\mathbf{q}} \omega_{\mathbf{q}} a_{\mathbf{q}}^\dagger a_{\mathbf{q}}\right\} \\ &= \exp\left\{-\frac{i\delta}{M} \sum_{\mathbf{q}} \omega_{\mathbf{q}} \left[\sum_{i=0}^{M-1} a_{\mathbf{q}}^{(i)\dagger} a_{\mathbf{q}}^{(i)} + \sum_{i \neq j=0}^{M-1} a_{\mathbf{q}}^{(i)\dagger} a_{\mathbf{q}}^{(j)} \right]\right\}, \end{aligned} \quad (27)$$

where U_0 is diagonal when acting on a state $|\psi\rangle$ in the representation discussed above. It can be written as multiplication by a phase factor,

$$U_0 |\psi\rangle = e^{-\frac{i\delta}{M} \sum_{\mathbf{q}} \omega_{\mathbf{q}} n_{\mathbf{q}}(1+n_\Omega)} |\psi\rangle = S_\varphi^{1+n_\Omega} |\psi\rangle, \quad (28)$$

where $S_\varphi \equiv \exp\{-i\frac{\delta}{M}\varphi\}$, $\varphi \equiv \sum_{\bar{\mathbf{n}}} \omega_{\mathbf{q}} n_{\mathbf{q}}$ is the total energy of all occupied states, and $n_{\mathbf{q}}$ (n_Ω) the number of registers with momentum \mathbf{q} (empty registers), while $\omega_{\mathbf{q}}$ is the continuum

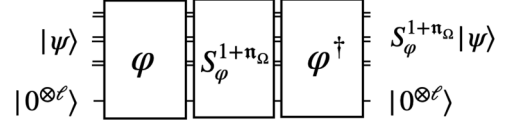


FIG. 4. Quantum circuit for U_0 , using $O(M \text{poly log}(\mathcal{V}))$ operations and 2ℓ ancilla qubits. Double lines indicate particle registers (including $|\mathbf{q}|$, sign, and occupation number qubits).

dispersion relation. The factor $n_{\mathbf{q}}(1+n_\Omega)$ reflects the two terms in the exponent of Eq. (27).

The algorithm for computing Eq. (28) is summarized in Fig. 4. It involves first computing the phase φ . This is done by the subcircuit depicted in Fig. 5, with two auxiliary registers of ℓ qubits. Here ℓ is determined by the precision of the algorithm to compute φ , $\boxed{+}$ is the quantum-addition operation [105,106] and we treat the circuit $\boxed{\omega}$ to compute $\omega_{\mathbf{q}}$ as a quantum “oracle.” The number of ancilla registers 2ℓ is determined by the precision with which we wish to compute $\omega_{\mathbf{q}}$ from \mathbf{q} . It should be taken to be similar to the number of qubits $\ell \sim O(\log(\mathcal{V})/d)$ that are necessary to realizing \mathbf{q} in one dimension. The number of gate operators included in $\boxed{\omega}$ is poly $\log(\mathcal{V})$. Efficient algorithms to compute simple arithmetic functions can be found in the literature [107–110].

Once φ is computed, one follows with $O(M)$ diagonal phase rotations $S_\varphi^{1+n_\Omega}$, using the occupation number qubits of each register as control qubits. (The detailed circuit is shown in Appendix C.) Finally, we uncompute $|\varphi\rangle$, so that in total we use $O(M)$ $\boxed{+}$ and $\boxed{\omega}$ gates. As a consequence, the algorithm for U_0 has an overall complexity of $O(M \text{poly log}(\mathcal{V}))$ gate operations per Trotter step.

2. Squeezing transformation

In order to implement the interaction piece of the time evolution operator U_I , we first perform a transformation from the single-particle representation in momentum space to position space. In a relativistic theory, single-particle states in position and momentum space are not simply Fourier conjugates. Therefore to obtain one from the other requires a combined squeezing operation [90] followed by a (quantum) Fourier transformation. To illustrate this, note that position space Fock operators are given by

$$a_{\mathbf{n}} \equiv \frac{1}{\sqrt{2}}(\phi_{\mathbf{n}} + i\pi_{\mathbf{n}}), \quad a_{\mathbf{n}}^\dagger \equiv \frac{1}{\sqrt{2}}(\phi_{\mathbf{n}} - i\pi_{\mathbf{n}}), \quad (29)$$

with the commutation relations $[a_{\mathbf{n}}, a_{\mathbf{n}'}^\dagger] = \delta_{\mathbf{n}, \mathbf{n}'}$, and the single-particle decomposition $a_{\mathbf{n}} \equiv \sum_i a_{\mathbf{n}}^{(i)}/\sqrt{M}$, $a_{\mathbf{n}}^\dagger \equiv \sum_i a_{\mathbf{n}}^{(i)\dagger}/\sqrt{M}$. We can define the Fourier conjugates $A_{\mathbf{q}}$ of $a_{\mathbf{n}}$ as

$$a_{\mathbf{n}} \equiv \frac{1}{\sqrt{\mathcal{V}}} \sum_{\mathbf{q}} A_{\mathbf{q}} e^{i2\pi \mathbf{n} \cdot \mathbf{q}/N_s}, \quad (30)$$

and likewise for their Hermitian conjugate counterparts. These are related [90] to the momentum space Fock operators $a_{\mathbf{q}}, a_{\mathbf{q}}^\dagger$ by

$$A_{\mathbf{q}} \equiv \frac{1}{2}[\omega_{\mathbf{q}}^{-\frac{1}{2}} + \omega_{\mathbf{q}}^{\frac{1}{2}}]a_{\mathbf{q}} + \frac{1}{2}[\omega_{\mathbf{q}}^{-\frac{1}{2}} - \omega_{\mathbf{q}}^{\frac{1}{2}}]a_{-\mathbf{q}}^\dagger, \quad (31)$$

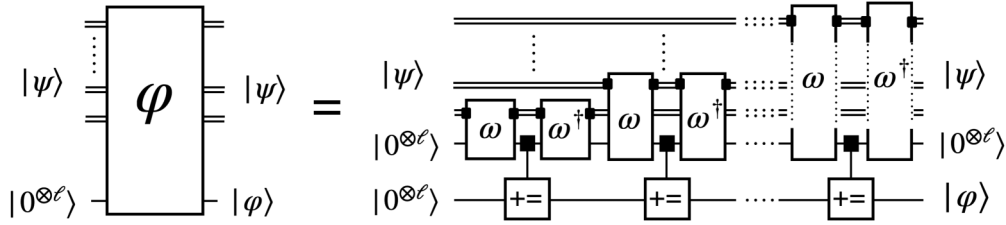


FIG. 5. Quantum circuit to compute φ , based on the algorithm in [111]. ω is an oracle to compute $\omega(\mathbf{q})$ for input $|\mathbf{q}\rangle$, and $\boxed{+=}$ is a quantum-addition circuit [105,106]. The \blacksquare symbol appearing in the gate $\boxed{+=}$ denotes that the associated register is an input into the gate. The relevant particle register input for the ω gates is denoted by (small) black boxes accordingly.

and likewise for $A_{\mathbf{q}}^\dagger$. Such squeezing operations are well known in quantum optics [89,112,113], where they are natural in the preparation of squeezed states. We will work out here their implementation on a digital quantum computer. To do so, note that Eq. (31) is realized by

$$A_{\mathbf{q}} = S a_{\mathbf{q}} S^\dagger, \quad A_{\mathbf{q}}^\dagger = S a_{\mathbf{q}}^\dagger S^\dagger, \quad (32)$$

where $S \equiv \prod_{\mathbf{q}} S_{\mathbf{q}}$, as shown in Fig. 6, and

$$S_{\mathbf{q}} \equiv \exp\{-z_{\mathbf{q}}[a_{\mathbf{q}}^\dagger a_{-\mathbf{q}}^\dagger - a_{-\mathbf{q}} a_{\mathbf{q}}]\}, \quad (33)$$

is a unitary operator with $z_{\mathbf{q}} \equiv \frac{1}{2} \log(\omega_{\mathbf{q}})$. See also Appendix D where we derive Eq. (31) from Eq. (32) and Eq. (33).

The circuit implementation of $S_{\mathbf{q}}$ is compactly summarized in Fig. 7. We can use a Trotter scheme to implement S , splitting the operation into \mathcal{V} modes \mathbf{q} and $M(M-1)/2$ steps over all possible register pairs $i \neq j$, $i, j = 0, \dots, M-1$, with a Trotter error of $O([n_{\mathbf{q}} z_{\mathbf{q}}/M]^2)$, where $n_{\mathbf{q}}$ is the occupation number of the mode \mathbf{q} of the state the operator acts on. We can then write

$$S = \prod_{\mathbf{q}, (i \neq j)} S_{\mathbf{q},ij} \quad (34)$$

and

$$S_{\mathbf{q},ij} \equiv \exp\left\{-\frac{z_{\mathbf{q}}}{M}[a_{\mathbf{q}}^{(i)\dagger} a_{-\mathbf{q}}^{(j)\dagger} - a_{-\mathbf{q}}^{(j)} a_{\mathbf{q}}^{(i)}]\right\}. \quad (35)$$

To implement $S_{\mathbf{q},ij}$, we decompose the single-particle Fock operators into spin raising and lowering operators (see Appendix A),

$$S_{\mathbf{q},ij} \equiv \exp\left\{-i\frac{z_{\mathbf{q}}}{M}\sigma_{\mathbf{q},ij}^y\right\}, \quad (36)$$

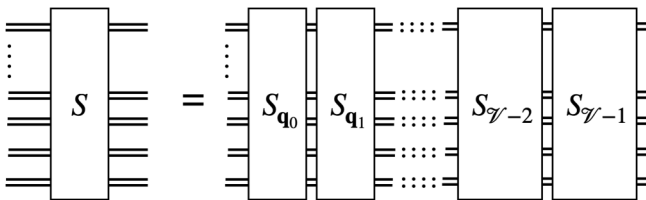


FIG. 6. Squeezing operator decomposition $S = \prod_{\mathbf{q}=q_0}^{q=q_{\mathcal{V}-1}} S_{\mathbf{q}}$. Notice that since creation and annihilation operators of different momentum modes commute, there is no Trotter error associated to this decomposition. See Eq. (33).

where $\sigma_{\mathbf{q},ij}^y \equiv (-i)[a_{\mathbf{q}}^{(i)\dagger} a_{-\mathbf{q}}^{(j)\dagger} - a_{-\mathbf{q}}^{(j)} a_{\mathbf{q}}^{(i)}]$. In the matrix representation of the \mathfrak{N} occupation and momentum qubits spanning $\{|\mathbf{q}\rangle \otimes |-\mathbf{q}\rangle, |\Omega\rangle \otimes |\Omega\rangle\}$, this can be written as

$$\sigma_{\mathbf{q},ij}^y = \begin{pmatrix} 0 & \dots & 0 & -i \\ 0 & \ddots & & 0 \\ \vdots & & \ddots & \vdots \\ i & 0 & \dots & 0 \end{pmatrix} \equiv \sigma_{\mathfrak{N}}^y. \quad (37)$$

Following a similar strategy as in [114], we block-diagonalize $\sigma_{\mathfrak{N}}^y$, using the (periodic) binary increment operator $I_{\mathfrak{N}} (I_1 = \sigma^x)$

$$I_{\mathfrak{N}}^\dagger \sigma_{\mathfrak{N}}^y I_{\mathfrak{N}} = \begin{pmatrix} 0 & \dots & \dots & 0 \\ \vdots & 0 & & 0 \\ \vdots & & \ddots & i \\ 0 & 0 & -i & 0 \end{pmatrix} \equiv \tilde{\sigma}_{\mathfrak{N}}^y. \quad (38)$$

The binary increment operator is a simple circuit and can be found in the literature (for example, in Fig. 2 of [114]), and is given explicitly in Appendix D. The recursion relation

$$\tilde{\sigma}_{\mathfrak{N}}^y = \frac{1}{2}(1 - \sigma^z) \otimes \tilde{\sigma}_{\mathfrak{N}-1}^y, \quad (39)$$

where $\tilde{\sigma}_1^y = -\sigma^y$, allows us to write

$$\tilde{\sigma}_{\mathfrak{N}}^y = \left[\bigotimes_{i=2}^{\mathfrak{N}} \frac{1}{2}(1 - \sigma^z) \right] \otimes \tilde{\sigma}_1^y. \quad (40)$$

Because $(1 - \sigma^z)$ is diagonal, the problem reduces to diagonalizing $\tilde{\sigma}_1^y = -\sigma^y = -\bar{S}H\sigma^zH\bar{S}^\dagger$, using the Hadamard H and phase gate \bar{S} acting on one qubit. Consequently, we can

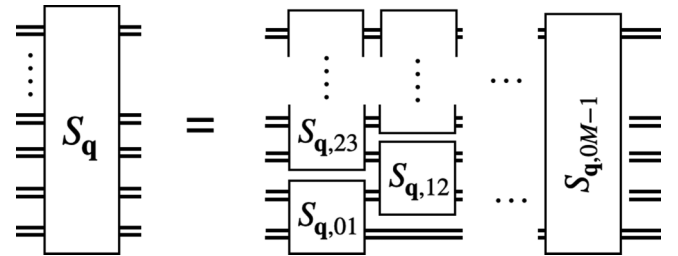


FIG. 7. Trotter decomposition of the squeezing operator S into $M(M-1)/2$ operations $S_{\mathbf{q},ij}$ ($i \neq j$). Note that because $S_{\mathbf{q},ij} = S_{\mathbf{q},ji}$, we can simplify $S_{\mathbf{q},ij}(z_{\mathbf{q}})S_{\mathbf{q},ji}(z_{\mathbf{q}}) = S_{\mathbf{q},ij}(2z_{\mathbf{q}})$.

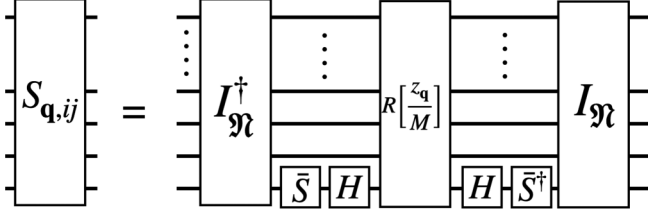


FIG. 8. Circuit implementation of $S_{q,ij}$ [Eq. (36)], using the bit-increment operator $I_{\mathfrak{N}}$ and the diagonal single qubit rotation $\exp\{i\frac{z_q}{M}\sigma^z\}$. It acts on the \mathfrak{N} qubits that make up $(-i)[a_q^{(i)\dagger}a_{-q}^{(j)\dagger} - a_{-q}^{(j)}a_q^{(i)}]$.

write

$$S_{q,ij} = I_{\mathfrak{N}} (1 \otimes \dots \otimes 1 \otimes H \bar{S}^\dagger) R\left[\frac{z_q}{M}\right] (1 \otimes \dots \otimes 1 \otimes \bar{S} H) I_{\mathfrak{N}}^\dagger, \quad (41)$$

where $R\left[\frac{z_q}{M}\right] \equiv \exp\{i\frac{z_q}{M}[\otimes_{i=2}^{\mathfrak{N}} \frac{1}{2}[1 - \sigma^z]_i] \otimes \sigma^z\}$ is a simple controlled (diagonal) σ^z -rotation. The algorithm is compactly summarized in Fig. 8.

The circuit implementation of the squeezing transformation contains $O(M^2 \mathcal{V} \text{poly}(\mathcal{V}))$ elementary gate operations per Trotter time step, where $\text{poly}(\mathcal{V})$ stands for the complexity of the bit increment $I_{\mathfrak{N}}$ and controlled z -rotation $R(z_q/M)$. The M^2 factor is due to iterations over pairs of particle registers, while \mathcal{V} reflects the operation being performed for all modes \mathbf{q} .

3. Quantum Fourier transform

Because the quantum Fourier transformation in Eq. (30) is a standard transformation and can be found in many textbooks [91], our discussion here will be brief. Within our digitization framework, it is performed separately for each register and dimension, conditional on whether the corresponding register is occupied. Towards this end, we first bring states [(13)–(17)] into a form where we can apply known algorithms for the symmetric quantum Fourier transform. This is done by first flipping the sign qubits which we then use to control σ^x -operations of all remaining qubits making up \mathbf{q}_i , $i = 1, \dots, d$. Interpreting the sign qubits as the major qubits of the decomposition of each \mathbf{q}_i , this allows us to apply the algorithm of [84], with $O(M \text{poly}(\mathcal{V}))$ elementary gate operations.

4. Interaction part U_I

We now turn to the final quantum circuit for the time evolution operator, that of the interaction term U_I . The ϕ^4 interaction term is local in position space and can be decomposed into \mathcal{V} Trotter steps per time step δ ,

$$U_I = \exp\left\{-i\delta \sum_{\mathbf{n}} \frac{\lambda}{4!} \phi_{\mathbf{n}}^4\right\} = \prod_{\mathbf{n}} \exp\left\{-i \frac{\delta \lambda}{4!} \phi_{\mathbf{n}}^4\right\} \equiv \prod_{\mathbf{n}} U_{I,\mathbf{n}}. \quad (42)$$

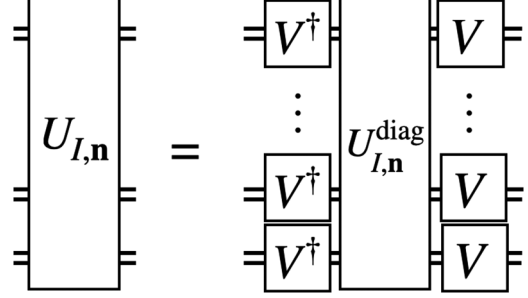


FIG. 9. Circuit implementation of $U_{I,\mathbf{n}}$. Double lines indicate particle registers. The operator $V \equiv V_{\mathbf{n}}^{(i)}$ ($i = 0, \dots, M-1$) is given in Eq. (46).

To implement the circuit for this operator, we write the field operator as $\phi_{\mathbf{n}} \equiv \sum_{i=0}^{M-1} \phi_{\mathbf{n}}^{(i)} / \sqrt{M}$, where

$$\phi_{\mathbf{n}}^{(i)} \equiv \frac{a_{\mathbf{n}}^{(i)} + a_{\mathbf{n}}^{(i)\dagger}}{\sqrt{2}} = \frac{1}{\sqrt{2}} \begin{pmatrix} 0 & \dots & 0 & 1 \\ 0 & \ddots & & 0 \\ \vdots & & \ddots & \vdots \\ 1 & 0 & \dots & 0 \end{pmatrix} \equiv \frac{1}{\sqrt{2}} \sigma_{\mathfrak{N}}^x, \quad (43)$$

with $\sigma_{\mathfrak{N}}^x$ being the \mathfrak{N} -qubit operator decomposition of $\phi_{\mathbf{n}}^{(i)}$, comprising the qubits that span $\{|\mathbf{n}\rangle, |\Omega\rangle\}$, as outlined in Appendix A. Following a similar strategy as before for the implementation of the squeezing operation in Sec. IV B 2, we write

$$U_{I,\mathbf{n}} \equiv V_{\mathbf{n}} U_{I,\mathbf{n}}^{\text{diag}} V_{\mathbf{n}}^\dagger, \quad (44)$$

where $U_{I,\mathbf{n}}^{\text{diag}}$ is a diagonal rotation matrix given by

$$U_{I,\mathbf{n}}^{\text{diag}} \equiv e^{-i\Delta \sum_{(i,j,k,l)} \phi_{\mathbf{n}}^{(i)\text{diag}} \phi_{\mathbf{n}}^{(j)\text{diag}} \phi_{\mathbf{n}}^{(k)\text{diag}} \phi_{\mathbf{n}}^{(l)\text{diag}}}, \quad (45)$$

with $\Delta \equiv \delta \lambda / (96M^2)$ and $V_{\mathbf{n}} \equiv \prod_{i=0}^{M-1} V_{\mathbf{n}}^{(i)}$ where

$$V_{\mathbf{n}}^{(i)} = I_{\mathfrak{N}} (1 \otimes \dots \otimes H). \quad (46)$$

Here $I_{\mathfrak{N}}$ is the bit-increment operator and H the Hadamard gate, while $\phi_{\mathbf{n}}^{(i)\text{diag}} \equiv V_{\mathbf{n}}^{(i)\dagger} \phi_{\mathbf{n}}^{(i)} V_{\mathbf{n}}^{(i)}$ satisfies $\phi_{\mathbf{n}}^{(i)\text{diag}} = \otimes_j \frac{1}{2}(1 - \sigma^z)_j \otimes \sigma^z$, in analogy to the previous section.

The algorithm to implement $U_{I,\mathbf{n}}$ is compactly summarized in Fig. 9, where $U_{I,\mathbf{n}}^{\text{diag}}$ can be realized using standard techniques for quantum simulation [91]. The exact form of $U_{I,\mathbf{n}}^{\text{diag}}$ can be obtained by performing the summation over $\langle i, j, k, l \rangle$ in Eq. (45). There are five distinct cases in this sum: either the four particles' indices match, three indices match, two indices match, two pairs of indices match independently or they all differ; to exemplify how this summation is carried out, we explicitly compute $U_{I,\mathbf{n}}^{\text{diag}}$ for $M = 4$ and $\mathbf{n} = -1/2$ in Appendix E.

The algorithm for U_I involves $O(M^4 \mathcal{V} \text{poly}(\mathcal{V}))$ elementary gate operations. The M^4 dependence originates from the need to account for all the possible ways to form four-tuples with M particles and reflects the brute force approach detailed in Appendix E. This bound can be lowered [presumably down to $O(M)$], provided one finds an efficient algorithm to deal with the combinatorics in computing the respective

phases by summing over (i, j, k, l) ; unfortunately we have not been able to construct such a simplified algorithm thus far. The linear dependence on volume is due to the fact that one has to loop over all positions while performing, for each one, $O(\text{poly} \log(\mathcal{V}))$ gate operations.

The Trotter complexity of the single-particle algorithm presented scales linearly with volume, similar to that of the field-operator-based strategy in [45,55,84]. A meaningful comparison between the approaches will depend on the problem under consideration. Determining the precision required to quantum simulate a simple scattering process, including taking the continuum limit, both in terms of the qubit representation of states and in the accuracy of the time evolution operator, will require a detailed numerical study using larger systems.

Moreover, error mitigation techniques [91,115] need to be applied should one attempt a quantum simulation with presently available devices. This is particularly important for the scheme presented because the size of the unphysical Hilbert space of non-Bose-symmetric states grows with M . This is similar to the problem of quantum simulating gauge theories where simulation errors may drive the system away from the physical Hilbert space defined by the Gauss law. It has been suggested that one can detect such violations of symmetries without compromising the information encoded in the system and thereby correct for them [116–120].

C. Measurement

In the spacetime picture of S -matrix scattering developed thus far, we first discussed the preparation of wave packets in the interacting theory by adiabatically turning on the interaction over a timescale τ_0 . After this timescale, the wave packets overlap and interact over a timescale τ_I , determined given by their spatial overlap. We will discuss here the algorithm for the measurement process subsequent to the scattering.

After the scattering, the wave function of the system can be written in the most general form¹⁴

$$\begin{aligned} |\Psi(t)\rangle &= \sum_{\ell} \alpha_{\ell}(t) |\Psi_{\ell}\rangle \\ &\equiv \sum_{\text{basis states}} \frac{\alpha_{(\mathbf{q}, \mathbf{q}', \dots)}(t)}{\sqrt{\mathcal{N}_{(\mathbf{q}, \mathbf{q}', \dots)}(t)}} [|\mathbf{q}, \mathbf{q}', \dots, \Omega\rangle + \text{symm}], \end{aligned} \quad (47)$$

with unknown coefficients $\alpha_{(\mathbf{q}, \mathbf{q}', \dots)}(t)$. Here “symm” denotes Bose-symmetric permutations and $\mathcal{N}_{(\mathbf{q}, \mathbf{q}', \dots)} \equiv M! / [n_{\Omega}! \prod_{\mathbf{q}} n_{\mathbf{q}}!]$ is a generalization of the Bose-symmetric factor \mathcal{N} introduced in Sec. IV A for the M single-particle registers, now also accounting for the possibility of degenerate momenta among particle registers.

Upon measurement of all qubits,¹⁵ the wave function in Eq. (47) will collapse to a state with well-defined particle number for every mode \mathbf{q} (a Fock state) with probability $|\alpha_{(\mathbf{q}, \mathbf{q}', \dots)}|^2$. Despite this, it is important to note that Eq. (47) does not imply any kind of localization or clustering of the particles measured in a detector, if measured at $t = \tau_0 + \tau_I$. One may further evolve the system over a time τ_f during which one turns off the interaction slowly to avoid interactions between separated wave packets¹⁶ until one ends up with localized particles over macroscopic scales that are theory specific. These are then straightforward to measure due to Eq. (47).

Measurements of identical Bose particles, with different orderings among the particle registers, are physically equivalent. Up to kinematic factors, this measurement defines the differential cross section

$$\frac{d^{dn} \sigma}{d^d \mathbf{p}_0 \dots d^d \mathbf{p}_n} \quad (48)$$

of $n = \sum_{\mathbf{q}} n_{\mathbf{q}}$ particles for a given outcome. From this perspective, running the quantum computer multiple times is very similar to accumulating events in an actual particle physics experiment, followed by a classical analysis of events. However, on the quantum computer, every outcome allowed by energy-momentum conservation, as well as other conserved quantities corresponding to symmetries of the system, is contained in the state (47). For example, one can simply measure only occupancy qubits, but not their corresponding momentum counterparts, to obtain an integrated cross section,

$$\sigma_n \equiv \int d^d \mathbf{p}_0 \dots d^d \mathbf{p}_n \frac{d^{dn} \sigma}{d^d \mathbf{p}_0 \dots d^d \mathbf{p}_n}, \quad (49)$$

directly. Similarly, in more complicated theories, one can introduce single-particle registers with qubits corresponding to electric charge, spin, or color and directly project on to desired values of these for a specific measurement.

One can also instruct the quantum algorithm to impose kinematical cuts such as measuring localized particle number in some region $\mathbf{p} \in [\mathbf{p}^{\min}, \mathbf{p}^{\max}]$. To achieve this, one requires $2d$ auxiliary registers [of size $\log_2(\mathcal{V})$] set to kinematic bounds $\mathbf{p}^{\min/\max}$ in d dimensions. One further requires a unitary comparator circuit [121–123] [using $\log_2(\mathcal{V})$ ancilla qubits and $O(\log(\mathcal{V}))$ gate operations] which computes whether $\mathbf{p}_i \leq \mathbf{p}_i^{\max}$ and $\mathbf{p}_i \geq \mathbf{p}_i^{\min}$ ($i = 1, \dots, d$) and stores the information in $2d$ ancilla qubits with outcome $|11\rangle^{\otimes 2d}$ if the momentum is within the kinematical range. This provides a way to efficiently split the Hilbert space into two nonoverlapping regions while tagging each component of the final state $|\Psi_I\rangle$ accordingly. As a consequence, techniques like (Oblivious) Amplitude Amplification [91,99–101,124,125] might be employed to boost the probability of measuring the rare final state that satisfies the kinematical cuts imposed. Alternately,

¹⁴The position space representation has an identical form and is used interchangeably in the forthcoming discussion. In fact, when we use the word “localized” here it can equally well mean “in position space,” albeit the formulas we give are in the momentum space representation.

¹⁵This is to be contrasted with the procedure in [44,45] where particle number measurement requires additional gate operations.

¹⁶Obviously, one can go beyond this picture by extracting information on the scattering process through measurements at *any* time, as we shall discuss below.

generalizing to other theories, one can use this method to identify states with unusual particle number content.

We note, however, that the regime at $\lambda = 0$, and that of its physical value, may not be adiabatically connected because the spectrum of the latter may consist of bound states. In this case, one omits the evolution over a time τ_f where one turns off the interaction and instead should keep the interaction time τ_l long enough to include the physical time it takes to form such a bound state. One example where the spectrum of the free and interacting theory are not adiabatically connected is that of QCD. While color-charged quark and gluon states arguably form a good basis to represent the proton wave function at high energies and short time intervals, at large distances and time intervals they are not contained in the physical spectrum because of the confinement and deconfinement phase transition, as is manifest in the dynamical process of hadronization and fragmentation between these regimes [126–129]. Such difficulties are also present in a field-based digitization, and explicit numerical analysis is required to investigate how well the proposed basis can approximate such states in the continuum limit.

As we discussed previously, the minimal timescale for the formation of a bound state is the Wigner time delay; for a discussion of resonance formation in the S -matrix picture, see [61]. Once this is done, and bound states are sufficiently separated, one can make local measurements of quantum numbers such as particle number or momentum (electric charge and spin can also be measured in more complicated theories, for example), the operator for the latter defined as

$$P_{\tilde{\mathcal{V}}_{\mathbf{p}}}^i \equiv \int_{\tilde{\mathcal{V}}_{\mathbf{p}}} d^d \mathbf{p} \mathbf{p}^i a_{\mathbf{p}}^\dagger a_{\mathbf{p}}, \quad (50)$$

where $i = 1, \dots, d$ and $\tilde{\mathcal{V}}_{\mathbf{p}}$ stands for a region in momentum space. Its expectation value can be obtained using variants of the phase estimation algorithm (PEA) [130–133]. The idea is to act on the state with $U \equiv \exp(-iP_{\tilde{\mathcal{V}}_{\mathbf{p}}}^i)$ to determine the operator expectation value $\langle P_{\tilde{\mathcal{V}}_{\mathbf{p}}}^i \rangle$. The PEA determines, with high probability, this expectation value to within precision ε . It requires extra $O(\log(\varepsilon^{-1})) \sim O(\log(\mathcal{V})/d)$ ancilla qubits¹⁷ and $O(\log(\varepsilon^{-1}))$ applications of the controlled- U operations. In our digitization scheme, it is straightforward to obtain $\langle P_{\tilde{\mathcal{V}}_{\mathbf{p}}}^i \rangle$ because the circuits of Sec. IV B 1 can be applied with small modifications. Concretely, one replaces $\omega_{\mathbf{p}}$ by \mathbf{p}^i in this algorithm and also uses a comparator circuit to check if \mathbf{p}^i is in $\tilde{\mathcal{V}}_{\mathbf{p}}$ controlling the execution of the circuit.

Likewise, the energy operator, restricted to $\tilde{\mathcal{V}}_{\mathbf{p}}$, is

$$H_{\tilde{\mathcal{V}}_{\mathbf{p}}} \equiv \int_{\tilde{\mathcal{V}}_{\mathbf{p}}} d^d \mathbf{p} H_{\mathbf{p}} = \int_{\tilde{\mathcal{V}}_{\mathbf{p}}} d^d \mathbf{p} H_{0,\mathbf{p}} + \int_{\tilde{\mathcal{V}}_{\mathbf{p}}} d^d \mathbf{p} H_{l,\mathbf{p}}, \quad (51)$$

where $H_{0,\mathbf{p}}$ and $H_{l,\mathbf{p}}$ are the Fourier transforms of the Hamiltonian densities $H_{0,\mathbf{x}}$ and $H_{l,\mathbf{x}}$, with $H_0 = \int d^d \mathbf{x} H_{0,\mathbf{x}}$ and $H_l = \int d^d \mathbf{x} H_{l,\mathbf{x}}$. One can measure the contribution to the expectation value $\langle H_{\tilde{\mathcal{V}}_{\mathbf{p}}} \rangle$ from the first term just as in Eq. (50). To

obtain the second term, we write

$$\int_{\tilde{\mathcal{V}}_{\mathbf{p}}} d^d \mathbf{p} H_{l,\mathbf{p}} = \int d^d \mathbf{p} H_{l,\mathbf{p}} \theta_{\tilde{\mathcal{V}}_{\mathbf{p}}}(\mathbf{p}), \quad (52)$$

where $\theta_{\tilde{\mathcal{V}}_{\mathbf{p}}}(\mathbf{p})$ is a (smooth) envelope function restricting the integrand to $\tilde{\mathcal{V}}_{\mathbf{p}}$. To illustrate the procedure, we now assume for simplicity that $\theta_{\tilde{\mathcal{V}}_{\mathbf{p}}}(\mathbf{p})$ is a sharp envelope function, e.g., a d -dimensional box function with equal length, i.e., $\theta_{\tilde{\mathcal{V}}_{\mathbf{p}}}(\mathbf{p}) = 1$ if $\mathbf{p} \in \tilde{\mathcal{V}}_{\mathbf{p}}$ and zero otherwise, where $\tilde{\mathcal{V}}_{\mathbf{p}} \equiv (L_{\mathbf{p}})^d$ is centered at some $\tilde{\mathbf{p}}$. We can make use of the Fourier convolution theorem to compute this term. First, using the momentum space translation operator introduced in Sec. IV A, we translate the state such that $\tilde{\mathcal{V}}_{\mathbf{p}}$ is centered around zero. After performing the squeezing and Fourier transformations discussed in Secs. IV B 2 and IV B 3, Eq. (52) can be written as

$$\int d^d \mathbf{x} H_{l,\mathbf{x}} g(-\mathbf{x}), \quad (53)$$

where the Fourier transform of the box function (centered around zero) is real, $g(\mathbf{x}) \equiv (2\pi)^{d/2} \prod_{i=1}^d \frac{\sin(x_i L_{\mathbf{p}}/2)}{x_i}$. The PEA [130–133] can be applied again, replicating the algorithm of Sec. IV B 4, albeit with the replacement $\lambda \rightarrow \lambda g(-\mathbf{x})$. For this specific envelope function, the measurement has a gate complexity of $O(\mathcal{VM}^4 \text{poly} \log(\mathcal{V}))$. A sharp envelope function is not ideal because it requires evaluating also the side-bands of the $\sin(x)/x$ function. In practice, one should use a smooth cutoff function, whose Fourier transform is known analytically or numerically, which falls off exponentially. In this case, the estimate will depend only on the much smaller subvolume $\mathcal{V}_x \subset \mathcal{V}$ over which the Fourier transform of the envelope function is supported, instead of the full volume \mathcal{V} . Similar algorithms are applied to compute energy and momentum densities restricted in position space.

In general, being able to control the wave function of a many-body system at any time t one can in principle follow the entire spacetime evolution of a particular collision system, instead of measuring just its asymptotic outcome, and thereby obtain snapshots of the collision process. This is important for systems such as ultrarelativistic heavy ion collisions where the primary interest lies in the thermalization and hydrodynamization of the produced matter [25] as opposed to the asymptotic final states. Likewise, following Feynman's idea of quantum simulating a particle physics experiment in its entirety, having full control over the time evolution allows one to measure arbitrary (nonequal time) correlation functions directly. (See also [134] where this point is discussed.) This will allow for a more direct comparison with current theoretical efforts such as computing parton distribution functions [38] or hadronic and Compton scattering amplitudes [70] from correlation functions.

Moreover, quantum computation allows one to address the question of entanglement in nuclear physics [135] and in high-energy physics. With regard to the latter, the single-particle basis described here may be useful to quantify entanglement between partons as probed in DIS experiments [136–139], its role in thermalization of the quark-gluon plasma, in hadronization [140–142], or in the composition of the proton's spin [143,144].

¹⁷We require that the precision of the PEA should be the same as that for the momentum space discretization.

D. Renormalization

The renormalization of quantum fields to absorb the apparent infinities that appear in computations is a fundamental feature of quantum field theories. It is therefore important to understand how to treat this problem in the real time Hamiltonian description of the evolution of quantum fields and its implementation on a quantum computer. More specifically, we need to understand how to implement the renormalization group for scattering problems in our single-particle framework.

We begin our discussion with a general overview of the renormalization group procedure in the Hamiltonian formalism. We will illustrate this picture in perturbation theory. We argue, however, that nonperturbative renormalization is essential to ensure one does not vitiate the reduction in computational complexity presented by quantum computations relative to classical approaches. We will therefore outline a concrete nonperturbative scheme closely paralleling the corresponding procedure in classical lattice computations in the (Euclidean) path integral formalism.

1. Operator formulation

The renormalization of quantum fields and operators requires finding a Hamiltonian for the effective field theory of interest (defined with an ultraviolet cutoff) concretely through a lattice discretization as well as the truncation of the Hilbert space imposed by a given digitization scheme. Since renormalization in the Hamiltonian operator formalism has been developed extensively [145], as well as its applications to single-particle strategies [146–148], we will outline only the relevant ideas in the context of this work. Working in the computational basis (the eigenbasis of the free Hamiltonian H_0) introduced in Sec. III, we can write the Hamiltonian in the block form

$$H = \begin{pmatrix} H_{ll} & H_{lh} \\ H_{hl} & H_{hh} \end{pmatrix}. \quad (54)$$

The matrix elements in this representation are between states with energies $E = \sum_{\mathbf{p}} \omega_{\mathbf{p}} n_{\mathbf{p}}$, either below (l) or above (h) a cutoff Λ .

A renormalization group (RG) transformation consists of the similarity transformation

$$H^{\text{eff}} \equiv THT^\dagger, \quad (55)$$

where $T \equiv \exp(i\eta)$ block-diagonalizes H , eliminating matrix elements between the low- and high-energy sectors such that H_{ii}^{eff} in the new basis defines a low-energy effective field theory.¹⁸ The generator η of this similarity transformation is not known *a priori*. It can, however, be constructed to realize a nonperturbative RG, the so-called similarity RG [145], by integrating out one energy shell at a time in infinitesimal steps. This point is discussed further in Appendix F.

If the coupling is small enough, perturbative renormalization is applicable. This procedure is very familiar to the high-energy physicist in its Lorentz covariant path integral formulation; in the Hamiltonian operator picture, it is best illustrated through a Schrieffer-Wolf transformation, as discussed in [150] and worked out in Appendix F. As is shown there, this allows us to systematically derive low-energy elements of H_{eff} and of any other operator order by order in λ .

However, it is not difficult to see that doing so comes with a factorial increase in the computational complexity, just as the number of Feynman diagrams grows factorially with loop order in a path integral formulation. Moreover such a perturbative computation will break down if there is a phase transition in λ , as is likely for $D = 2, 3$ for scalar ϕ^4 theory; for QCD, this expansion will be problematic for quantum simulations that attempt to treat hadronization of parton single-particle degrees of freedom.

Therefore to match the quantum advantage of the renormalization procedure with that of the nonperturbative formulation of the rest of our treatment of the scattering problem, we will outline below a practical scheme to nonperturbatively renormalize the theory on a quantum computer.

2. Nonperturbative renormalization scheme

We begin by outlining how exactly renormalization enters our algorithm. As shown in Fig. 1, the algorithm includes a turn-on of interactions from a free (but unphysical) theory at $t = 0$, where the initial state can be prepared, to the interacting (physical) theory at $t = \tau_0$ with time-dependent Hamiltonian $H(t) = H(\lambda(t), m(t))$.

It is only the couplings in the physical Hamiltonian at $t \geq \tau_0$,

$$\lambda(\tau_0) = \lambda^{\text{ren}}, \quad m(\tau_0) = m^{\text{ren}}, \quad (56)$$

that are to be determined by a renormalization group procedure which we outline below. The “unphysical” theories defined by $H(t) = H(\lambda(t), m(t))$ at $t < \tau_0$, including the initial values

$$\lambda(0) = 0, \quad m(0) = m_0, \quad (57)$$

are not renormalized because there is simply no physical renormalization for them. Instead, one simply works with a linear interpolation

$$\lambda(t) = \lambda^{\text{ren}} \frac{t}{\tau_0}, \quad m(t) = m_0 \left(1 - \frac{t}{\tau_0}\right) + m^{\text{ren}} \frac{t}{\tau_0}, \quad (58)$$

for $t \in [0, \tau_0]$ and constant thereafter. From a practical perspective, the unknown parameter m_0 may be chosen to represent a relevant energy scale in the weakly coupled regime of the theory such as, for example, the bare quark mass in QCD. However, if the system undergoes a phase transition during this turn-on procedure, the mass and energy scales of the weakly and strongly coupled regimes of the theory are very different (as is the case in QCD), requiring large lattices to resolve both regimes.

We now turn our attention to determining the renormalized values for the bare parameters $\lambda(t)$ and $m(t)$ at $t \geq \tau_0$. We will assume form invariance of the Hamiltonian of the form (11) for all values of lattice spacing a_s and particle number cutoff

¹⁸Note that a self-consistent formulation of the S -matrix in this picture may provide deeper insight into ambiguities regarding the elementarity of the degrees of freedom included in the EFT [61]. For a recent discussion, see [149].

M . In other words, we do not add dimensionful operators that would be generated by the similarity transformation in Eq. (55). (These could in principle improve the convergence to the continuum limit.)

To renormalize the Hamiltonian operator, it is sufficient to perform the computation of a static property and then use the result as the input for the computation of a scattering process.¹⁹ The nonperturbative renormalization strategy consists of the following steps:

(1) First, one quantum computes a static and dimensionless physical quantity such as the energy ratio of two low-lying excitations at a given a_s and M . One then repeats the computation adjusting the bare parameters λ , m so that the physical value is reproduced for that a_s and M . We will not discuss the details of such computations here but note that algorithms²⁰ to do so can be applied to our single-particle digitization.

(2) One then repeats the computation at a somewhat different a_s , M along the direction $a_s \rightarrow 0$ and $M \rightarrow \infty$, and adjusts the values of λ , m so that the aforementioned physical quantity does not change.

(3) One repeats this computation for various a_s , M along a line of constant physics. Because there are now two directions (a_s, M) , this procedure is in principle ambiguous. In practice, however, it should be subject to an optimization procedure identifying the most relevant RG direction, such as determined by a steepest decent approach. We will not discuss such a procedure here.

(4) Once the renormalized values λ^{ren} and m^{ren} are known for a range of (a_s, M) , one performs the scattering experiment outlined in this paper with these values as input. This also includes the renormalization of operators $\langle O^{\text{eff}} \rangle$ measured in Sec. IV C such as particle number, momentum, and energy density. In the simplest case, one sets $O = ZO^{\text{eff}}$ and determines Z in the same way as for the bare λ and m .

(5) Finally, one performs a continuum extrapolation of the observables obtained in the scattering experiment. This dynamical problem will require determining the λ^{ren} , m^{ren} , and Z over a large range (a_s, M) , which is likely computationally demanding even with a quantum computer.

This procedure is similar to the Luscher formalism that relates energy differences between static long-lived states and S -matrix elements. Extracting the latter from the former is in general an inverse scattering problem and a number of sophisticated techniques have been developed in this regard [157]. A potential advantage of the quantum computation is that both sides of the Luscher relation can be computed in real time; realizing this in practice is of course very challenging.

V. SUMMARY AND OUTLOOK

In this work, we developed a single-particle digitization strategy for the quantum simulation of scattering in a relativistic scalar ϕ^4 field theory in d dimensions. The essence of this picture is a relativistic generalization of a single-particle picture consisting of M “particle registers” whose Hilbert space spans states over a volume \mathcal{V} . Our approach is nonperturbative and fully general and may offer a quantum advantage over other digitization strategies for a class of interesting physical problems that are challenging to address with purely classical methods.

The conceptual elements of this framework are outlined in Secs. II and III. We developed quantum circuits for the initial state preparation of scattering wave packets in Sec. IV A, their time evolution through the scattering process in Sec. IV B, and the subsequent measurement of final states in Sec. IV C. We sketched in Sec. IV D the elements of a nonperturbative renormalization strategy that must be implemented in the quantum simulation to achieve physically meaningful results.

The overall gate complexity of the elements of a quantum circuit for a scattering simulation are compactly summarized in Table I. The initial state preparation requires $O(M^n \log(\mathcal{V}))$ elementary gate operations, where n is the initial number of particles (the simplest case being two-particle scattering with $n = 2$), and $O(\log(M^n))$ ancilla qubits. The algorithm may become probabilistic, requiring additional measurements for certain choices of n and M depending on Bose combinatorics. A Trotter scheme is employed to separate the time evolution operator into free and interaction parts; these are evaluated respectively in momentum and position space representations of the single-particle digitization basis. The change of basis from the former to the latter is achieved through a combination of squeezing and quantum Fourier transform operations. The dominant cost of the algorithm is from the $O(M^4 \mathcal{V} \text{poly log}(\mathcal{V}))$ gate operations per Trotter step required to compute the interaction part of the time evolution operator. We believe that one can improve the polynomial cost in the number of registers M by improving the algorithm outlined in Sec. IV B 4. This would open up a broader class of interaction terms and theories that could be efficiently simulated within this approach. The measurement of particle number incurs no additional cost; the estimation of the localized momentum and energy density (in a subvolume $\mathcal{V}_x \subset \mathcal{V}$), via the phase estimation algorithm, requires $O(M \text{poly log}(\mathcal{V}))$ and $O(M^4 \mathcal{V}_x \text{poly log}(\mathcal{V}))$ operations, respectively. We note that some of the unitary operations in our circuit, such as the squeezing operation or the diagonal phase multiplication used in computing the ϕ^4 interaction term, are available as native gates in certain architectures such as circuit QED [158], potentially improving their resource efficiency and facilitating a near-term implementation of our strategy.

Apart from the Hilbert space truncation, sources of errors in our algorithm are from the Trotterization of the time evolution operator, and imperfect evolution of the qubits on non-error-corrected devices. It should be possible to derive rather tight bounds on the Trotter error, using similar techniques as in [159], and it would be interesting to compare them with [44,45]. Machine errors, such as bit flips, are important because, if they occur in a major bit of the momentum

¹⁹A caveat here is that since the scattering process likely covers a larger range of scales, the continuum extrapolation of the cross section is more challenging than that of the low-energy spectrum.

²⁰Examples of such algorithms include variational approaches [151,152], adiabatic state preparation with quantum phase estimation [153,154], quantum approximate optimization [151,155], quantum imaginary time and quantum Lanczos algorithms [156], and efficient operator averaging techniques [130–133].

TABLE I. Cost of the circuit implementation discussed in this manuscript, assuming noiseless qubits. We use the following abbreviations: number of particle registers M , volume \mathcal{V} , occupied registers in initial state n , dimension d , and Trotter time steps t . (*) If $\log_2(M!/(M-n))$ cannot be chosen integer, the initial state is prepared with probability $p_{\text{success}} > 1/2$, depending on the choice of M and n . (**) Measurements of (localized) energy and momentum densities are via the phase estimation algorithm (PEA) [130–133]. The cost estimate for the localized energy density includes a factor $\mathcal{V}_x \subset \mathcal{V}$ denoting a small subvolume of the total \mathcal{V} ; see Sec. IV C.

		Elementary gate operations	Ancilla qubits
Initial state preparation	$O(M^n \log(\mathcal{V}))$	$p_{\text{success}} = 1$ [exact*] $p_{\text{success}} > 1/2$ [probabilistic*]	$\log[M!/(M-n!)]$ [exact*] $O(\log(M^n))$ [probabilistic*]
Time evolution	Free part U_0	$O(M \text{poly} \log(\mathcal{V}) t)$	$O(\log(\mathcal{V})/d)$
	Squeezing transform S	$O(M^2 \mathcal{V} \text{poly} \log(\mathcal{V}) t)$	0
	Quantum Fourier transform	$O(M \text{poly} \log(\mathcal{V}) t)$	0
	Interaction part U_I	$O(M^4 \mathcal{V} \text{poly} \log(\mathcal{V}) t)$	$O(\log(\mathcal{V})/d)$
	Total	$O(M^4 \mathcal{V} \text{poly} \log(\mathcal{V}) t)$	$O(\log(\mathcal{V})/d)$
Measurement	Particle number	0	0
	Momentum density	$O(M \text{poly} \log(\mathcal{V}))$ (PEA**)	$O(\log(\mathcal{V})/d)$
	Energy density	$O(M^4 \mathcal{V}_x \text{poly} \log(\mathcal{V}))$ (PEA**)	$O(\log(\mathcal{V})/d)$

or position of a particle register, they can change a position or momentum eigenstate drastically. Such errors could be protected using linear codes [160–162]. We also note that, because the momentum or position information is entangled over several registers in our (Bose-symmetric) digitization, such errors will take the state into an unphysical regime and can be detected easily. Whether this symmetry can be used to correct or minimize errors will be explored in future work.

Our framework can be compared to the paradigmatic description of scattering on quantum computers by Jordan, Lee, and Preskill (JLP) [44,45] which, in contrast, is based on the digitization of field operators.²¹ Our digitization strategy differs fundamentally from JLP and other field digitization approaches since the number of degrees of freedom in our approach scales linearly with the particle number (and as a logarithm of the volume) as opposed to the linear scaling with volume in the field digitization approach. However, the logarithmic scaling in our approach holds only if the system is dilute; for dense systems with high occupancy, one recovers linear scaling or greater with the volume and the single-particle strategy is no longer preferred. This is seen on the algorithmic level when the required Bose or Fermi symmetrization creates a large overhead of unphysical or unused states in Hilbert space. Because $M \sim \mathcal{V}$ in such situations, the cost for the time evolution operator would be significantly higher, albeit still polynomial in volume, as can be inferred from Table I.

The situation is analogous to the virial expansion we discussed previously which breaks down for high-density systems. Thus just as the virial expansion is very useful for a wide class of many-body problems, our single-particle approach may present a quantum advantage for a number of physical problems. From a purely practical point of view, the logarithmic scaling with volume of our approach will be useful in benchmark computations for a class of scattering

problems with NISQ era quantum hardware, where only few tens to hundreds of noisy qubits will be available. A physics application where our strategy may provide a quantum advantage is the Feynman diagram approach to compute scattering amplitudes at weak coupling. As pointed out in [44,45] a quantum computation avoids the combinatorial complexity with increasing precision that burdens classical computations. Another appealing feature of our strategy is the relative simplicity of initial state preparation and of the extraction of inclusive cross sections; the latter, for instance, requires no additional gate operations. Not least, the single-particle approach, as articulated in Sec. IV D, provides a transparent realization of a nonperturbative renormalization scheme that can simultaneously be used to fix lattice masses and couplings from comparisons to static properties of the system and to compute physically meaningful cross sections.

One can extend our strategy to fermionic theories and theories involving internal symmetries. For a fermionic theory, the algorithm in Sec. IV A can be modified to produce antisymmetrized wave functions and may offer a new fermion qubit mapping that is useful in higher dimensions. Internal symmetries such as spin and color can also be realized via the strategy discussed in [31]. For example, to realize a Dirac fermion in $3+1$ dimensions, one needs only to modify Eq. (14) to include two extra fermionic degrees of freedom; these can then be mapped on to two qubits by means of a Jordan-Wigner transformation, thereby realizing the four-dimensional spinor matrix space. Likewise, for color $SU(3)$ in the fundamental representation, only three extra qubits are required. Details of the spin and extensions to $SU(N_c)$ in arbitrary representations are given in [31,134,144].

The theory can be nonperturbatively coupled to gauge fields.²² An important consequence in doing so is that the quadratic term of the Hamiltonian, whose implementation is discussed in Sec. IV B 1, is not diagonal anymore. The theory can be nonperturbatively coupled to gauge fields. An important consequence in doing so is that the quadratic term

²¹The implementation of the JLP program for scattering problems has been discussed at length recently [84] and compared to an alternative digitization strategy employing a harmonic oscillator basis in position or momentum space [90,163,164].

²²For discussions of first principles quantum simulation of non-Abelian gauge theories see [165–171].

of the Hamiltonian, whose implementation is discussed in Sec. IV B 1, is not diagonal anymore. Hence one would have to develop an algorithm similar to that used for the interaction term. A significant downside would be that one no longer can work with the continuum dispersion relation in momentum space but would instead have to use a lattice discretization of the Laplacian operator in Eq. (11). This introduces larger discretization errors which are unknown in the strongly coupled regime and are likely more severe than the cost of the squeezing and quantum Fourier transformations that are avoided by working purely in the coordinate space basis.

As a next step, we aim to perform a numerical study focusing on the simplest case of $d = 1$ spatial dimensions. While we work in the eigenbasis of the free Hamiltonian, we will test, using exact diagonalization, how well the spectrum of the theory can be reproduced in the interacting theory at finite λ for given lattice discretization and M . This is similar to what is done in [84] using the digitization of [44,45]. At weak coupling, the results of such study can be compared with lattice perturbation theory, unlike at strong coupling where the analysis includes varying M and \mathcal{V} over a wider range, hoping for eventual convergence.

Next, one could classically compute our algorithm within the simplest case of $M = 2$ in $d = 1$ dimensions with $N_s = 8$ (16) lattice sites. This would correspond to a quantum simulation with 8 (10) qubits, plus an overhead of ancilla qubits. An important motivation for such a study would be to quantify the consequences of the violation of Bose symmetry by injecting errors into the simulation.

With this as benchmark, we plan to implement elements of our circuit on available quantum hardware, starting in the simplest case of $M = 2$ in $d = 1$ dimensions, which we assume can be done using lattices up to $N_s \sim O(8)$ sites. While negligible for large systems, the overhead from ancilla qubits is a significant part of the computational budget for such a small number of sites. Preparing the Bose-symmetrized initial state is already a nontrivial task involving entangling the two particle registers. To implement the time evolution algorithm, a quantum algorithm for the oracle to compute the single-particle energy $\omega_{\mathbf{q}}$ from the momentum \mathbf{q} has to be devised for the free part of the time evolution operator U_0 . While it is certainly possible to come up with an efficient circuit for $\omega_{\mathbf{q}}$, a simpler strategy would be to simulate U_0 in position space albeit with a lattice discretized Laplacian operator. The resulting complexity of $O(\mathcal{V})$ versus $O(\log(\mathcal{V}))$ would hardly make a difference on lattices this small.

Finally, we should mention that we see important applications of our single-particle basis digitization strategy to quantum computing scattering cross sections, nuclear structure functions and jet fragmentation functions probed at high-energy collider experiments such as the Large Hadron Collider, the Relativistic Heavy Ion Collider and the upcoming Electron-Ion Collider [172]. A single-particle basis may also be useful to quantify the role of entanglement in high-energy and nuclear physics, for example, between partons probed in DIS experiments [136–139], the evolution of entanglement during the parton fragmentation process [140,141] and its role in the composition of the proton’s spin [143]. We also see novel applications of this approach [49,173] to systems in high-energy nuclear and particle physics that can

be described by hybrid quantum and classical dynamics such as QCD in the Regge limit [82] and the thermalization dynamics of the quark-gluon plasma in ultrarelativistic heavy ion collisions [25,174–176].

ACKNOWLEDGMENTS

N.M. would like to thank Ning Bao, Zohreh Davoudi, Nikhil Karthik, Alex Shaw, and Torsten Zache for discussions. R.V. would like to thank Robert Konik for a useful discussion. We also thank Nathan Wiebe for very useful comments on quantum algorithms. This project was supported by a fellowship to J.B. from “la Caixa” Foundation (ID 100010434), fellowship code LCF/BQ/DI18/11660057, and by funding from the European Union’s Horizon 2020 research and innovation program under the Marie Skłodowska-Curie Grant Agreement No. 713673. J.B. is supported by Ministerio de Ciencia e Innovacion of Spain under project FPA2017-83814-P; Unidad de Excelencia Maria de Maetzu under project MDM-2016-0692; European Research Council project ERC-2018-ADG-835105 YoctoLHC; and Xunta de Galicia (Conselleria de Educacion) and FEDER. J.B. also acknowledges the support from the Fulbright Commission and the hospitality of Brookhaven National Laboratory. N.M. acknowledges funding by the Deutsche Forschungsgemeinschaft (DFG, German Research Foundation), Project 404640738, and by the U.S. Department of Energy, Office of Science, Office of Nuclear Physics, under Contract No. DE-SC0012704 while at Brookhaven National Lab where a significant part of the work presented was performed, and by the U.S. Department of Energy’s Office of Science, Office of Advanced Scientific Computing Research, Accelerated Research in Quantum Computing program award DE-SC0020312. The work of A.T. is supported by the U.S. Department of Energy, Office of Science, Office of Nuclear Physics under Award No. DE-SC0004286 and in part by the joint BNL/Stony Brook Center for Frontiers in Nuclear Science (CFNS). This material is based upon the work of R.V. supported by the U.S. Department of Energy, Office of Science, National Quantum Information Science Research Centers under the “Co-design Center for Quantum Advantage” award. The work of R.V. is also supported by the U.S. Department of Energy, Office of Science, Office of Nuclear Physics, under Contract No. DE-SC0012704.

APPENDIX A: SINGLE-PARTICLE DIGITIZATION SCHEME

In this Appendix, we provide additional details on the single-particle digitization strategy introduced in Sec. III, based on mapping single-particle states to a chain of spins (14)–(16), where

$$a_{\mathbf{q}}^{\dagger} \equiv \frac{1}{\sqrt{M}} \sum_{i=0}^{M-1} a_{\mathbf{q}}^{(i)\dagger}, \quad (\text{A1})$$

and similarly for $a_{\mathbf{q}}$. Here $a_{\mathbf{q}}^{(i)\dagger}$, $a_{\mathbf{q}}^{(i)}$ are “hard-core boson” creation (annihilation) operators which can be written as a product of spin raising (lowering) operators $S^{\pm} = 1/2(\sigma^x \pm i\sigma^y)$. A simple example is a digitization with $N = 4$ qubits per

particle register in $d = 1$ dimensions, where there are eight “occupied” states with $\mathbf{q} \in [-7/2, 7/2]$,

$$\begin{aligned} |\pm 1/2\rangle &\equiv |\downarrow\downarrow; \uparrow/\downarrow; \uparrow\rangle, & |\pm 3/2\rangle &\equiv |\downarrow\uparrow; \uparrow/\downarrow; \uparrow\rangle, \\ |\pm 5/2\rangle &\equiv |\uparrow\downarrow; \uparrow/\downarrow; \uparrow\rangle, \\ |\pm 7/2\rangle &\equiv |\uparrow\uparrow; \uparrow/\downarrow; \uparrow\rangle, \end{aligned} \quad (\text{A2})$$

and the empty state $|\Omega\rangle = |\downarrow\downarrow; \downarrow; \downarrow\rangle$. Fock operators are then

$$\begin{aligned} a_{-1/2}^{(i)\dagger} &\equiv S_0^+, & a_{-3/2}^{(i)\dagger} &\equiv S_2^+ S_0^+, \\ a_{-5/2}^{(i)\dagger} &\equiv S_3^+ S_0^+, & a_{-7/2}^{(i)\dagger} &\equiv S_3^+ S_2^+ S_0^+, \end{aligned} \quad (\text{A3})$$

where $a_{\pm|\mathbf{q}|}^{(i)\dagger} = S_1^+ a_{\mp|\mathbf{q}|}^{(i)\dagger}$. We label the $k = 0, \dots, 3$ qubits from right to left so that $k = 0$ labels the occupation number qubit, $k = 1$ the sign qubit and $k = 2, 3$ are the binary decomposition of $|\mathbf{q}|$. We use the identical map for states in the position representation.

One can check that $a_{\mathbf{q}}^{(i)\dagger} |\Omega^{(i)}\rangle = |\mathbf{q}^{(i)}\rangle$ and $(a_{\mathbf{q}}^{(i)\dagger})^2 = (a_{\mathbf{q}}^{(i)})^2 = 0$. Using Eq. (A1), one can also show that $[a_{\mathbf{q}}^\dagger, a_{\mathbf{q}'}^\dagger] = [a_{\mathbf{q}}, a_{\mathbf{q}'}] = 0$ and

$$[a_{\mathbf{q}}, a_{\mathbf{q}}^\dagger] = \frac{1}{M} \sum_{i=0}^{M-1} [\{a_{\mathbf{q}}^{(i)}, a_{\mathbf{q}}^{(i)\dagger}\} - 2a_{\mathbf{q}}^{(i)\dagger} a_{\mathbf{q}}^{(i)}] = 1 + O\left(\frac{n_{\mathbf{q}}}{M}\right), \quad (\text{A4})$$

where 1 is a unit matrix in the space spanned by $|\mathbf{q}\rangle$ and $|\Omega\rangle$, as well as $[a_{\mathbf{q}}, a_{\mathbf{q}'}^\dagger] = O(n_{\mathbf{q}}/M)$ where $n_{\mathbf{q}}$ is the occupation number of the mode \mathbf{q} .

APPENDIX B: DETAILS OF STATE PREPARATION

We will present here details of the initial state preparation algorithm in Sec. IV A. We begin by discussing the preparation of a wave packet superposition via the algorithm of [101,102] and contrast it with a simpler, albeit less general, variant. For simplicity, we work in $d = 1$, and use the standard binary representation, not the “inverted” one used in the main text. Assuming a symmetric distribution in momentum, the first Hadamard operation on the sign qubit creates an equal superposition of negative and positive momenta. Below we illustrate the algorithm acting on the qubits representing the absolute value of momentum p .

Starting from a fiducial state with all the qubits in $|0\rangle$, our algorithm applies the (per qubit) operation²³

$$|0\rangle \rightarrow \cos \theta_k |0\rangle + \sin \theta_k |1\rangle \quad (\text{B1})$$

for all $k = 0, \dots, n_Q - 1$ qubits, so that to each $|1\rangle$ gets multiplied with a sine and to each $|0\rangle$ with a cosine. Then the final state (for n_Q qubit) reads

$$\begin{aligned} |0, 0, \dots, 0\rangle &\rightarrow \sum_{p=0}^{2^{n_Q}-1} \left\{ \prod_{k=0}^{n_Q-1} [\cos^{(1-p_k)}(\theta_k) \sin^{(p_k)}(\theta_k)] \right\} |p\rangle \\ &= \sum_{p=0}^{2^{n_Q}-1} \psi_p |p\rangle \equiv |\Psi\rangle, \end{aligned} \quad (\text{B2})$$

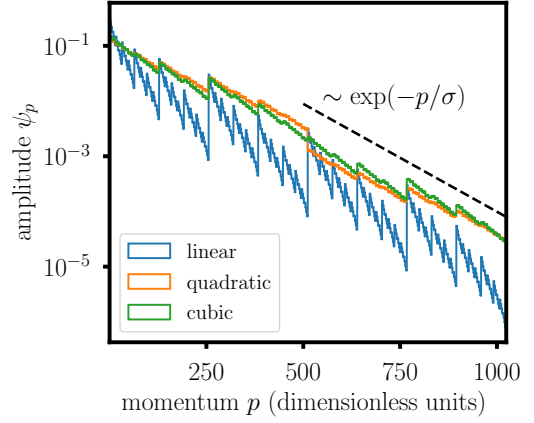


FIG. 10. Induced distributions for ψ_p using the above polynomial maps. For comparison, we additionally plot an off-set exponentially decaying distribution, with $\sigma = 100$.

where $|p\rangle$ here stands for the n_Q qubits storing the absolute value of a single particle and $p_k \in \{0, 1\}$.

Adjusting the map $k \rightarrow \theta_k$ classically, one can reproduce a wide range of distributions. For example, choosing $\theta_k = \pi/4$ up to some k' and $\theta_k = 0$ thereafter would produce a step function. While this distribution is localized (in momentum space), its Fourier conjugate is $\sin(x)/x$ (in position space), which falls off only polynomially, and is thus undesired.

One can, however, produce sufficiently smooth distributions that fall off exponentially in position and momentum space. Simple examples of this are shown in the figure below, where for illustration we have chosen the following maps:

$$\theta_k^{\text{linear}} = \frac{\pi}{4} - \epsilon + \frac{2\epsilon - \frac{\pi}{4}k}{n_Q - 1}, \quad (\text{B3})$$

$$\theta_k^{\text{quadratic}} = \frac{\pi}{4} - \epsilon + \left[2\epsilon - \frac{\pi}{4} - c_0(n_Q - 1)^2 \right] \frac{k}{n_Q - 1} + c_0 k^2, \quad (\text{B4})$$

$$\begin{aligned} \theta_k^{\text{cubic}} &= \frac{\pi}{4} - \epsilon + \left[2\epsilon - \frac{\pi}{4} - c_1(n_Q - 1)^2 - c_2(n_Q - 1)^3 \right] \\ &\times \frac{k}{n_Q - 1} + c_1 k^2 + c_2 k^3. \end{aligned} \quad (\text{B5})$$

The c_i parameters are adjusted such that the resulting distribution is smoothed (in the sense of having less and smaller peaks); we took $c_0 = -0.01325$, $c_1 = -0.0195$, $c_2 = 0.0005905$, the numerical regulator $\epsilon = 0.015$ and $n_Q = 10$. These maps are fixed at the initial point $p = 0$ where $\theta_0 = \pi/4 - \epsilon$ and $\theta_{n_Q-1} = \epsilon$ is the smallest possible value. The resulting distributions decay exponentially, $\sim \exp(-p/\sigma)$ as was desired. We note that the use of these simple low order polynomials leads to a roughness of the curves, which can be smoothed by use of higher order polynomials as is shown in Fig. 10.

While the analytic maps (B3)–(B5), which we worked out with pen and paper, provide some insight, in practice one would use a (classical) numerical optimization procedure to determine the optimal map, without assuming a functional form, for a given target distribution. In this case, the difference of our approach to that of [101,102] is that the angles θ_k are

²³We now work in the standard binary representation.

determined simultaneously (“globally”) while in [101,102] they are determined sequentially (the latter also requiring controlled operations). Our motivation for this “classical outsourcing” was the relative simplicity of our approach over that of [101,102] in light of available near-term resources. However, being satisfied with our approach producing distributions relevant for our problem, we do not know if it is also capable of producing more general distributions realizable with [101,102]

We continue here with details of the Bose-symmetrization procedure discussed in Sec. IV A. The idea behind the algorithm is to start from an unsymmetrized state, work out all permutations of particle registers that together give the symmetrized state (a simple combinatorial problem) and then use an ancilla register in a Bell superposition. Every state in this superposition is interpreted as the binary representation of a number labeling the respective Bose permutations of the initial unsymmetrized state. Each combination may then be used as the control qubits to execute a unique swap operation.

A simple but nontrivial example is the case of $n = 2$ initial wave packets in $M = 3$ registers, where the Bose-symmetrized state, obtained from the initial unsymmetrized state $|\Omega, \Psi_1, \Psi_0\rangle$, reads

$$\frac{1}{\sqrt{6}}[|\Omega, \Psi_1, \Psi_0\rangle + |\Omega, \Psi_0, \Psi_1\rangle + |\Psi_0, \Psi_1, \Omega\rangle + |\Psi_1, \Psi_0, \Omega\rangle + |\Psi_0, \Omega, \Psi_1\rangle + |\Psi_1, \Omega, \Psi_0\rangle]. \quad (\text{B6})$$

Following the recipe given in the main text, the number of possible Bose permutation for this M and n is not a power of two. Using $s = 3$ ancilla qubits in a Bell superposition in fact gives $2^3 = 8$ different permutations. Because of this the following state is generated:

$$\begin{aligned} & |\Omega, \Psi_1, \Psi_0\rangle \\ & \rightarrow \frac{1}{\sqrt{8}}[|\Omega, \Psi_1, \Psi_0\rangle |0, 0, 0\rangle + |\Omega, \Psi_0, \Psi_1\rangle |0, 0, 1\rangle \\ & \quad + |\Psi_0, \Psi_1, \Omega\rangle |1, 0, 0\rangle + |\Psi_1, \Psi_0, \Omega\rangle |1, 0, 1\rangle \\ & \quad + |\Psi_0, \Omega, \Psi_1\rangle (|0, 1, 1\rangle + |1, 1, 0\rangle) \\ & \quad + |\Psi_1, \Omega, \Psi_0\rangle (|0, 1, 0\rangle + |1, 1, 1\rangle)], \end{aligned} \quad (\text{B7})$$

where states $|\Psi_0, \Omega, \Psi_1\rangle$ and $|\Psi_1, \Omega, \Psi_0\rangle$ are now twice as likely as any other state. These unwanted permutations can be eliminated by introducing a single ancilla $|0\rangle$, and flipping it to $|1\rangle$ if either $|1, 1, 0\rangle$ or $|1, 1, 1\rangle$ is detected by a simple controlled σ^x gate. If the ancilla is then measured in the $|0\rangle$ state, Eq. (B7) collapses onto Eq. (B6) with probability given by ratio of the number of desired terms in Eq. (B7) to the total number of states, in this specific example $p_{\text{success}} = 6/8$.

Note that although the number of basic gate operations depends on the number of measurements one needs to perform in order to eliminate all undesired states—in the previous example at least two— p_{success} depends only on $\{n, M\}$. In the example above, if each of the two undesired states had been eliminated separately, the probability of preparing the correct symmetrized state would be $p_{\text{success}} = (7/8) \times (6/7) = 6/8$, as promised. In general, it is easily recognized that

$$p_{\text{success}} = \frac{\mathcal{N}}{2^s} > \frac{1}{2}, \quad (\text{B8})$$

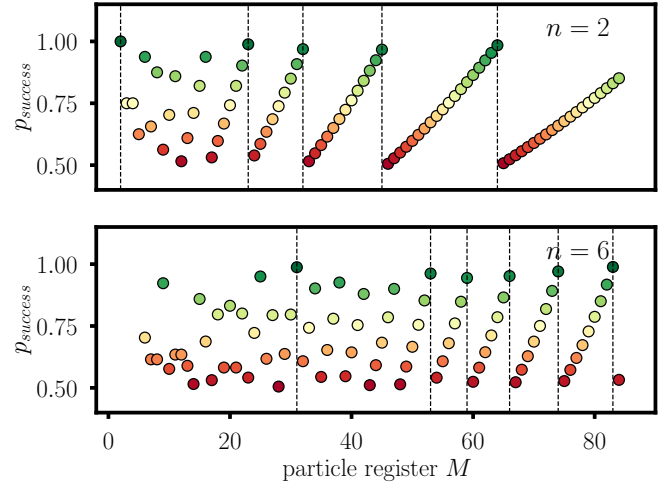


FIG. 11. Probability of preparing the correct Bose symmetric state p_{success} as a function of the number for single-particle registers M , for $n = 2$ (top) and $n = 6$ (bottom) initial single-particle states. The graduation in color between red and green is to guide the eye from low (≈ 0.5) to high (≈ 1.0) success probability; vertical dashed lines indicate values of M that maximize p_{success} .

with $\mathcal{N} = M!/(M - n)!$ the number of Bose permutations one needs to generate and s an integer such that 2^s is the closest power of two to \mathcal{N} from above, $s = \lceil \log_2(M!/(M - n)!) \rceil = O(\log(M^n))$.

In Fig. 11 we give some values for $n = 2$ and $n = 6$ as a function of M , with 6 being the number of “particles” one would need to represent the quantum numbers of the proton in an extension of this work. Shown is the total probability of success for given choices of M , with the graduation in color from red to green guiding the eye from low (≈ 0.5) to high (≈ 1.0) probability. One would like to choose M as large as possible, to minimize truncation effects, but this may not always be possible due to limited resources. However, as indicated by vertical dashed lines, one can always choose M optimally in a reasonable range, so that p_{success} is maximized.

The next step is to uncompute the s ancilla qubits, as described in the main text. For $n = 2$ this can be done using the occupation number qubit, as well as sign qubit, because the initial wave packets have opposite momentum in order to be able to interact. The major difference for $n > 2$ is that it is not sufficient to use only sign and occupation number qubits alone to uncompute the ancilla qubits. In this case, one must also use r of the qubits making up the momentum \mathbf{q} (or position \mathbf{x} after the respective transformation). Because the wave packets are assumed widely separated, a small number of qubits should suffice to uncompute the ancillas. The cost of uncomputing the ancillas would increase from $O(M^n)$, to $\sim O(M^n r) \ll O(M^n \log(\mathcal{V}))$, where $r \ll \log_2(\mathcal{V})$ is the number of qubits representing the momentum/position of each wave packet which differ uniquely from each other. One then uncomputes the $s' \leq s$ ancillas that are in the $|1\rangle$ state. Since one can choose s' to be very small (compared to s) its contribution to the overall scaling estimate is subleading. Overall, the algorithm uses s Hadamard gates to prepare the ancilla register, and $O(2^s \log \mathcal{V}) \sim O(M^n \log \mathcal{V})$ controlled swap operations,

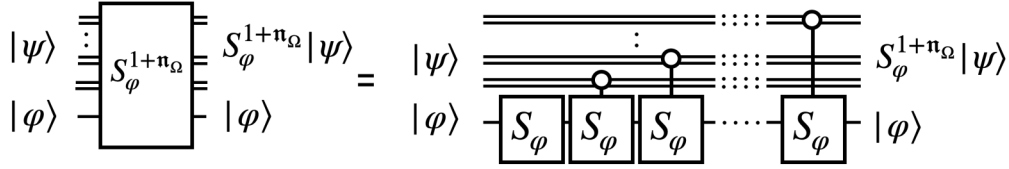


FIG. 12. Circuit implementing the final step in the time evolution dictated by H_0 . The first S_ϕ gate contributes with S_ϕ to the phase, while the last M gates contribute only if controlled by a particle register in the vacuum state, thus generating the term proportional to n_Ω in the phase.

and the uncomputation of the ancilla register requires $O(M^n)$ operations; the overall gate complexity is $O(M^n \log \mathcal{V})$.

APPENDIX C: DETAILS OF THE KINETIC TERM

In this Appendix, we discuss the implementation of the gates ω and $S_\phi^{1+n_\Omega}$, necessary for the algorithm introduced in Sec. IV B. The gate ω takes as an input two registers, one of which is a particle register $|\mathbf{q}\rangle$ and the other an ancilla register of l qubits in the state $|0^{\otimes l}\rangle$. Under the action of this gate, the state $|\mathbf{q}\rangle \otimes |0^{\otimes l}\rangle$ transforms to $|\mathbf{q}\rangle \otimes |\omega_{\mathbf{q}}\rangle$. Assuming that an efficient classical algorithm exists to compute $\omega_{\mathbf{q}}$ for any \mathbf{q} , and ensuring that for $|\Omega\rangle$, $\omega_\Omega = 0$ (using the occupation number qubit as control), we treat ω as a quantum oracle. The gate implementing Eq. (28) is given in Fig. 12 and consists of the sequential application of single controlled gates S_ϕ which takes the state $|\psi\rangle \otimes |\phi\rangle$ to $\exp(-i\frac{\delta}{M}\varphi)|\psi\rangle \otimes |\phi\rangle$.

This set of operations uses conditional single qubit phase shift gates C_ϕ [91,177], with matrix representation

$$C_\phi \equiv \begin{pmatrix} 1 & 0 \\ 0 & e^{i\phi} \end{pmatrix}, \tag{C1}$$

where $\phi = -\frac{\delta}{M}2^d$ ($0 \leq d \leq l - 1$) chosen accordingly to the binary decomposition of φ . The full multiqubit gate is constructed as a product of single qubit gates.

APPENDIX D: DETAILS OF THE SQUEEZING TRANSFORMATION

In this Appendix we will show that the operator S realizes Eq. (31). First, note that

$$S a_{\mathbf{q}} S^\dagger = \prod_{\mathbf{p}, \mathbf{p}'} e^{-z_{\mathbf{p}}(a_{\mathbf{p}}^\dagger a_{-\mathbf{p}}^\dagger - a_{-\mathbf{p}} a_{\mathbf{p}})} a_{\mathbf{q}} e^{z_{\mathbf{p}'}(a_{\mathbf{p}'}^\dagger a_{-\mathbf{p}'}^\dagger - a_{-\mathbf{p}'} a_{\mathbf{p}'})}. \tag{D1}$$

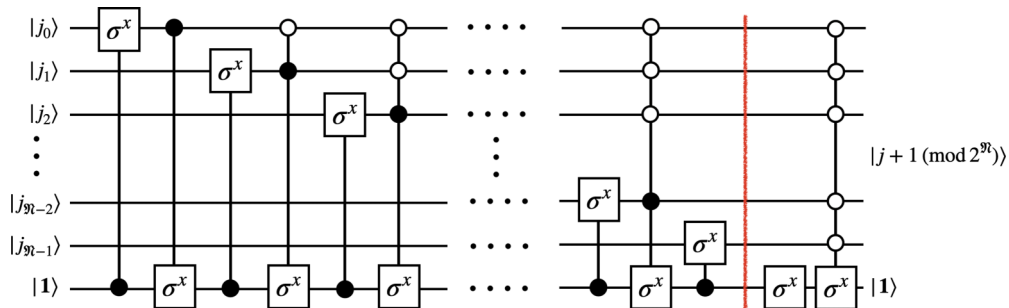


FIG. 13. Circuit implementing the bit increment operator $I_{\mathfrak{N}}$, introduced by Kaye [178,179]. The number of elementary quantum gate operations required scales as $O(\mathfrak{N}^2)$ for $\mathfrak{N} \geq 3$, leading to the polylogarithm scaling mentioned in the main text.

Taking into account that $a_{\mathbf{p}}$ and $a_{\mathbf{p}}^\dagger$ obey the canonical commutation relations, Eq. (D1) takes the form

$$e^X a_{\mathbf{q}} e^{-X} = \sum_{k=0}^{\infty} \frac{1}{k!} \underbrace{[X, [X, \dots [X, a_{\mathbf{q}}]] \dots]}_{k \text{ times}}, \tag{D2}$$

where $X \equiv -z_{\mathbf{q}}(a_{\mathbf{q}}^\dagger a_{-\mathbf{q}}^\dagger - a_{-\mathbf{q}} a_{\mathbf{q}})$. Using the simple identities

$$[X, a_{\mathbf{q}}] = z_{\mathbf{q}} a_{-\mathbf{q}}^\dagger, \quad [X, a_{-\mathbf{q}}^\dagger] = z_{\mathbf{q}} a_{\mathbf{q}}, \tag{D3}$$

it follows directly that for $z_{\mathbf{q}} < 0$,

$$\begin{aligned} e^X a_{\mathbf{q}} e^{-X} &= \sum_{k=0}^{\infty} \frac{(z_{\mathbf{q}})^{2k}}{(2k)!} a_{\mathbf{q}} + \sum_{k=0}^{\infty} \frac{(z_{\mathbf{q}})^{2k+1}}{(2k+1)!} a_{-\mathbf{q}}^\dagger \\ &= \cosh(z_{\mathbf{q}}) a_{\mathbf{q}} + \frac{z_{\mathbf{q}}}{|z_{\mathbf{q}}|} \sinh(z_{\mathbf{q}}) a_{-\mathbf{q}}^\dagger. \end{aligned} \tag{D4}$$

In the implementation of the squeezing operation introduced in the main text, we made use of the bit increment operator $I_{\mathfrak{N}}$, that performs the transformation $|j\rangle \rightarrow |j + 1 \pmod{2^{\mathfrak{N}}}\rangle$, where $|j\rangle = |j_0, j_1, \dots, j_{\mathfrak{N}-2}, j_{\mathfrak{N}-1}\rangle$ and $j_i \in \{0, 1\}$ for any i . A decomposition of $I_{\mathfrak{N}}$ in terms of usual quantum gates is given in Fig. 13; an alternative formulation is given in Eq. (47) of [114].

The implementation of $I_{\mathfrak{N}}$ in terms of Fig. 13 uses the fact that unitary increments in the binary basis consist in consecutively flipping all qubits, i.e., $|0\rangle \rightarrow |1\rangle$ and $|1\rangle \rightarrow |0\rangle$, while keeping track of the first time the state $|0\rangle$ is given as an input qubit. To do this, a flag ancilla qubit is prepared in the $|1\rangle$ state and it is flipped back to $|0\rangle$ only just after one performs the transformation $|0\rangle \rightarrow |1\rangle$ (on an input qubit); all possible remaining qubit flips are skipped. This operation is performed by the circuit detailed to the left of the vertical red line in Fig. 13. In the end, one uncomputes the ancilla back to the state $|1\rangle$ via a single σ^x gate. The special (boundary) case $|1, 1, \dots, 1\rangle \otimes |1\rangle \rightarrow |0, 0, \dots, 0\rangle \otimes |1\rangle$ has the ancilla uncomputed by the last gate in the diagram shown.

APPENDIX E: DETAILS OF THE INTERACTION TERM

In this Appendix, we will discuss how to explicitly construct the operator $U_{I,\mathbf{n}}^{\text{diag}}$. We illustrate the algorithm for the simplest example $\mathbf{n} = -1/2$ and $M = 4$. The generalization for all \mathbf{n} and M is discussed below.

For this simple example, $\phi_{-1/2}^{(i)\text{diag}}$ is simply the σ^z operator acting only on the occupancy qubit of register i ; see Eq. (A3). For $M = 4$, $U_{I,-1/2}^{\text{diag}}$ acts only on the respective occupancy qubits of the four particle registers. Using the fact that $(\sigma^z)^2 = 1$, we can write $U_{I,-1/2}^{\text{diag}}$ as

$$U_{I,-1/2}^{\text{diag}} \equiv \exp \left\{ -i\Delta \sum_{s=0}^2 c_{s,-1/2} \mathcal{O}_{s,-1/2} \right\}. \quad (\text{E1})$$

The three distinct operators appearing in Eq. (E1) are $\mathcal{O}_{0,-1/2} = 1^{\otimes 4}$, $\mathcal{O}_{1,-1/2} = (\sigma^z)^{\otimes 4}$, and $\mathcal{O}_{2,-1/2} = \mathcal{P}_{\Sigma}(1 \otimes 1 \otimes \sigma^z \otimes \sigma^z)$, with coefficients $c_{0,-1/2} = 4!(4 + 12)$, $c_{1,-1/2} = 4!$ and $c_{2,-1/2} = 4!(2 + 1)$. Here $\mathcal{P}_{\Sigma}(\hat{X})$ stands for the sum over all permutations of the operator \hat{X} in the tensor product. Each operator is simply a product of standard Pauli z -rotations [91]. The generalization of Eq. (E1) to arbitrary \mathbf{n} (and M) requires replacing σ^z by its higher dimensional analog, given in Sec. IV B 4. For $M > 4$ one has to repeat the algorithm for all $M(M-1)(M-2)(M-3)/4! \sim O(M^4)$ possible four-tuples formed out of M registers.

APPENDIX F: DETAILS OF THE RENORMALIZATION PROCEDURE

In this Appendix, we present some details of the renormalization procedure. Concretely, for weak coupling Eq. (55) can be expanded as

$$H^{\text{eff}} = H + [i\eta, H] + \frac{1}{2!}[i\eta[i\eta, H]] + \dots = H_0 + H_I + [i\eta, H_0] + [i\eta, H_I] + \frac{1}{2}[i\eta, [i\eta, H_0]] + O(\lambda^3), \quad (\text{F1})$$

where $H = H_0 + H_I$ and $H_I \sim O(\lambda)$, $\eta \sim O(\lambda)$. We label eigenstates $H_0|\alpha, i\rangle = E_{\alpha,i}|\alpha, i\rangle$, where $\alpha = l, h$ denote low- and high-energy sectors (the computational basis states of Sec. III). To block-diagonalize H such that $\langle \alpha, i | H^{\text{eff}} | \beta, j \rangle = 0$ if $\alpha \neq \beta$, we require that the diagonal elements of $i\eta$ vanish, $\langle \alpha, i | i\eta | \alpha, j \rangle = 0$, and we set $\langle \alpha, i | i\eta | \beta, j \rangle = \langle \alpha, i | H_I | \beta, j \rangle / (E_{\alpha,i} - E_{\beta,j})$ for $\alpha \neq \beta$. With this, the off-diagonal elements of H^{eff} cancel to $O(\lambda^2)$. In this case, $H^{\text{eff}} = H_0 + H_I + \frac{1}{2}[i\eta, H_I] + O(\lambda^3)$, with the low-energy matrix elements given by

$$\langle l, i | H_{\text{eff}} | l, j \rangle = \langle l, i | H | l, j \rangle + \frac{1}{2} \sum_k \langle l, i | H_I | h, k \rangle \langle h, k | H_I | l, j \rangle \left[\frac{1}{E_{l,i} - E_{h,k}} + \frac{1}{E_{l,j} - E_{h,k}} \right]. \quad (\text{F2})$$

The same transformation applies to any operator $\mathcal{O}_{\text{eff}} = T \mathcal{O} T^\dagger$, which can be expressed as $\langle l, i | \mathcal{O}_{\text{eff}} | l, j \rangle = \langle l, i | \mathcal{O} | l, j \rangle + \langle l, i | \Delta \mathcal{O} | l, j \rangle$. For the matrix elements for an observable diagonal in the eigenbasis of H_0 (such as particle number), this reads as²⁴

$$\langle l, i | \Delta \mathcal{O} | l, j \rangle = \sum_k \left\{ \frac{\langle l, i | H_I | h, k \rangle \langle h, k | H_I | l, j \rangle}{E_{l,i} - E_{h,k}} \frac{1}{E_{h,l} - E_{l,j}} \frac{1}{2} [\mathcal{O}_j^l + \mathcal{O}_i^l] - \frac{\langle l, i | H_I | h, k \rangle \mathcal{O}_k^h \langle h, k | H_I | l, j \rangle}{E_{h,k} - E_{l,j}} \frac{1}{E_{l,i} - E_{h,k}} \right\}, \quad (\text{F3})$$

where we abbreviated $\langle l, i | \mathcal{O} | l, j \rangle \equiv \mathcal{O}_i^l \delta_{ij}$. The procedure outlined can in principle be continued to arbitrary order $O(\lambda^n)$.

The generalization of Eq. (F3) to an operator that is not diagonal in the H_0 eigenbasis is

$$\begin{aligned} \langle l, i | \Delta \mathcal{O} | l, j \rangle = & \sum_k \frac{\langle l, i | H_I | h, k \rangle}{E_{l,i} - E_{h,k}} \langle h, k | \mathcal{O} | l, j \rangle \langle l, i | \mathcal{O} | h, k \rangle \frac{\langle h, k | H_I | l, j \rangle}{E_{l,j} - E_{h,k}} + \frac{1}{2} \sum_{k,m} \left\{ \frac{\langle l, i | H_I | h, k \rangle \langle h, k | H_I | l, m \rangle}{E_{l,i} - E_{h,k}} \frac{1}{E_{h,k} - E_{l,m}} \langle l, m | \mathcal{O} | l, j \rangle \right. \\ & - \frac{\langle l, i | H_I | h, k \rangle}{E_{l,i} - E_{h,k}} \langle h, k | \mathcal{O} | h, m \rangle \frac{\langle h, m | H_I | l, j \rangle}{E_{h,m} - E_{l,j}} - \frac{\langle l, i | H_I | h, m \rangle}{E_{l,i} - E_{h,m}} \langle h, m | \mathcal{O} | h, k \rangle \frac{\langle h, k | H_I | l, j \rangle}{E_{h,k} - E_{l,j}} \\ & \left. + \langle l, i | \mathcal{O} | l, m \rangle \frac{\langle l, m | H_I | h, k \rangle \langle h, k | H_I | l, j \rangle}{E_{l,m} - E_{h,k}} \frac{1}{E_{h,k} - E_{l,j}} \right\}. \quad (\text{F4}) \end{aligned}$$

To generalize the renormalization procedure beyond weak coupling, one may use Wegner's formulation of an infinitesimal operator renormalization group [145] whereby states inside an energy shell of width δ around the cutoff Λ are integrated: $H(\Lambda - n\delta) = T(n)H(\Lambda)T^\dagger(n)$ with $T(n) = \exp *i\eta(n)$, $H(\Lambda - N\delta) = H^{\text{eff}}$ after a number of RG steps N , and $\eta(n) = [H_d(n), H(n)]$. Here $H_d(n)$ is the diagonal part of the Hamiltonian obtained after $n \leq N$ steps. The Hamiltonian $H(\Lambda \rightarrow \infty)$ is usually not known, and in practice one starts from an ansatz for H_I^{eff} at finite Λ , such as Eq. (11), and takes the continuum limit as described in Sec. IV D. Classical numerical procedures have been derived from Wegner's operator RG [182], and it would be interesting to explore their use in quantum computation.

²⁴This formalism is analogous to a Poisson bracket formalism invented in the context of weak wave turbulence in fluids [180]. Interestingly, it has been exploited recently to study the self-similar infrared behavior of a scalar ϕ^4 theory far-off-equilibrium [181].

- [1] J. D. Whitfield, J. Biamonte, and A. Aspuru-Guzik, *Mol. Phys.* **109**, 735 (2011).
- [2] I. Kassal, J. D. Whitfield, A. Perdomo-Ortiz, M.-H. Yung, and A. Aspuru-Guzik, *Annu. Rev. Phys. Chem.* **62**, 185 (2011).
- [3] P. J. O'Malley, R. Babbush, I. D. Kivlichan, J. Romero, J. R. McClean, R. Barends, J. Kelly, P. Roushan, A. Tranter, N. Ding *et al.*, *Phys. Rev. X* **6**, 031007 (2016).
- [4] C. Hempel, C. Maier, J. Romero, J. McClean, T. Monz, H. Shen, P. Jurcevic, B. P. Lanyon, P. Love, R. Babbush *et al.*, *Phys. Rev. X* **8**, 031022 (2018).
- [5] M. Lewenstein, A. Sanpera, V. Ahufinger, B. Damski, A. Sen, and U. Sen, *Adv. Phys.* **56**, 243 (2007).
- [6] I. Bloch, J. Dalibard, and S. Nascimbene, *Nat. Phys.* **8**, 267 (2012).
- [7] N. Bao, P. Hayden, G. Salton, and N. Thomas, *New J. Phys.* **17**, 093028 (2015).
- [8] U. R. Fischer and R. Schützhold, *Phys. Rev. A* **70**, 063615 (2004).
- [9] P. Jain, S. Weinfurter, M. Visser, and C. W. Gardiner, *Phys. Rev. A* **76**, 033616 (2007).
- [10] A. Chatrchyan, K. Geier, M. K. Oberthaler, J. Berges, and P. Hauke, [arXiv:2008.02290](https://arxiv.org/abs/2008.02290) (2020).
- [11] J. Carlson, D. J. Dean, M. Hjorth-Jensen, D. Kaplan, J. Preskill, K. Roche, M. J. Savage, and M. Troyer, Quantum computing for theoretical nuclear physics, a white paper prepared for the US Department of Energy, Office of Science, Office of Nuclear Physics, Tech. Rep. (USDOE Office of Science, Washington, DC, 2018).
- [12] A. J. McCaskey, Z. P. Parks, J. Jakowski, S. V. Moore, T. D. Morris, T. S. Humble, and R. C. Pooser, *npj Quantum Inf.* **5**, 99 (2019).
- [13] E. F. Dumitrescu, A. J. McCaskey, G. Hagen, G. R. Jansen, T. D. Morris, T. Papenbrock, R. C. Pooser, D. J. Dean, and P. Lougovski, *Phys. Rev. Lett.* **120**, 210501 (2018).
- [14] E. Rico, M. Dalmonte, P. Zoller, D. Banerjee, M. Bögli, P. Stebler, and U.-J. Wiese, *Ann. Phys.* **393**, 466 (2018).
- [15] I. C. Cloët, M. R. Dietrich, J. Arrington, A. Bazavov, M. Bishof, A. Freese, A. V. Gorshkov, A. Grassellino, K. Hafidi, Z. Jacob *et al.*, [arXiv:1903.05453](https://arxiv.org/abs/1903.05453) (2019).
- [16] K. Matchev, S. Mrenna, P. Shyamsundar, and J. Smolinsky, Quantum (2020), <https://snowmass21.org/docs/files/summaries/CompF/SNOWMASS21-CompF6-TF10-004.pdf>.
- [17] D. Kielpinski, C. Monroe, and D. J. Wineland, *Nature (London)* **417**, 709 (2002).
- [18] C. Monroe, *Nature (London)* **416**, 238 (2002).
- [19] A. Blais, R.-S. Huang, A. Wallraff, S. M. Girvin, and R. J. Schoelkopf, *Phys. Rev. A* **69**, 062320 (2004).
- [20] J. I. Cirac and P. Zoller, *Nat. Phys.* **8**, 264 (2012).
- [21] P. Hauke, F. M. Cucchietti, L. Tagliacozzo, I. Deutsch, and M. Lewenstein, *Rep. Prog. Phys.* **75**, 082401 (2012).
- [22] J. Preskill, *Quantum* **2**, 79 (2018).
- [23] A. Roggero and J. Carlson, *Phys. Rev. C* **100**, 034610 (2019).
- [24] A. Roggero, A. C. Y. Li, J. Carlson, R. Gupta, and G. N. Perdue, *Phys. Rev. D* **101**, 074038 (2020).
- [25] J. Berges, M. P. Heller, A. Mazeliauskas, and R. Venugopalan, [arXiv:2005.12299](https://arxiv.org/abs/2005.12299) [hep-th] (2020).
- [26] M. Breidenbach, J. I. Friedman, H. W. Kendall, E. D. Bloom, D. H. Coward, H. C. DeStaebler, J. Drees, L. W. Mo, and R. E. Taylor, *Phys. Rev. Lett.* **23**, 935 (1969).
- [27] J. D. Bjorken, *Phys. Rev.* **179**, 1547 (1969).
- [28] J. D. Bjorken and E. A. Paschos, *Phys. Rev.* **185**, 1975 (1969).
- [29] D. J. Gross and F. Wilczek, *Phys. Rev. Lett.* **30**, 1343 (1973).
- [30] J. Blumlein, *Prog. Part. Nucl. Phys.* **69**, 28 (2013).
- [31] N. Mueller, A. Tarasov, and R. Venugopalan, *Phys. Rev. D* **102**, 016007 (2020).
- [32] H. Lamm, S. Lawrence, Y. Yamauchi, N. Collaboration *et al.*, *Phys. Rev. Research* **2**, 013272 (2020).
- [33] M. Kreshchuk, W. M. Kirby, G. Goldstein, H. Beauchemin, and P. J. Love, [arXiv:2002.04016](https://arxiv.org/abs/2002.04016) (2020).
- [34] A. Bassetto, M. Ciafaloni, and G. Marchesini, *Phys. Rep.* **100**, 201 (1983).
- [35] Y. L. Dokshitzer, V. A. Khoze, S. Troian, and A. H. Mueller, *Rev. Mod. Phys.* **60**, 373 (1988).
- [36] A. Metz and A. Vossen, *Prog. Part. Nucl. Phys.* **91**, 136 (2016).
- [37] F. Winter, W. Detmold, A. S. Gambhir, K. Orginos, M. J. Savage, P. E. Shanahan, and M. L. Wagman, *Phys. Rev. D* **96**, 094512 (2017).
- [38] X. Ji, *Phys. Rev. Lett.* **110**, 262002 (2013).
- [39] C. Alexandrou, K. Cichy, V. Drach, E. Garcia-Ramos, K. Hadjiyiannakou, K. Jansen, F. Steffens, and C. Wiese, *Phys. Rev. D* **92**, 014502 (2015).
- [40] J.-W. Chen, S. D. Cohen, X. Ji, H.-W. Lin, and J.-H. Zhang, *Nucl. Phys. B* **911**, 246 (2016).
- [41] A. Radyushkin, *Phys. Lett. B* **767**, 314 (2017).
- [42] H.-W. Lin *et al.*, *Prog. Part. Nucl. Phys.* **100**, 107 (2018).
- [43] W. Detmold, R. G. Edwards, J. J. Dudek, M. Engelhardt, H.-W. Lin, S. Meinel, K. Orginos, and P. Shanahan (USQCD), *Eur. Phys. J. A* **55**, 193 (2019).
- [44] S. P. Jordan, K. S. Lee, and J. Preskill, [arXiv:1112.4833](https://arxiv.org/abs/1112.4833) (2011).
- [45] S. P. Jordan, K. S. Lee, and J. Preskill, *Science* **336**, 1130 (2012).
- [46] N. Klco and M. J. Savage, *Phys. Rev. A* **102**, 052422 (2020).
- [47] M. J. Strassler, *Nucl. Phys. B* **385**, 145 (1992).
- [48] B. Bauer, D. Wecker, A. J. Millis, M. B. Hastings, and M. Troyer, *Phys. Rev. X* **6**, 031045 (2016).
- [49] W. A. de Jong, M. Metcalf, J. Mulligan, M. Płoskoń, F. Ringer, and X. Yao, [arXiv:2010.03571](https://arxiv.org/abs/2010.03571) [hep-ph] (2020).
- [50] B. A. Lippmann and J. Schwinger, *Phys. Rev.* **79**, 469 (1950).
- [51] R. G. Newton, *Scattering Theory of Waves and Particles* (Springer Science & Business Media, Berlin-Heidelberg, Germany, 2013).
- [52] H.-D. Meyer, J. Horáček, and L. S. Cederbaum, *Phys. Rev. A* **43**, 3587 (1991).
- [53] E. P. Wigner and L. Eisenbud, *Phys. Rev.* **72**, 29 (1947).
- [54] K. Yeter-Aydeniz, G. Siopsis, and R. C. Pooser, [arXiv:2008.08763](https://arxiv.org/abs/2008.08763) [quant-ph] (2020).
- [55] S. P. Jordan, K. S. M. Lee, and J. Preskill, *Quantum Inf. Comput.* **14**, 1014 (2014).
- [56] J. Dorfman, T. R. Kirkpatrick, and J. V. Sengers, *Annu. Rev. Phys. Chem.* **45**, 213 (1994).
- [57] J. Dorfman, T. R. Kirkpatrick, and J. V. Sengers, *Advances in the Computational Sciences* (World Scientific, 2017), pp. 24–51, Chap. 3.
- [58] K. Huang and C. N. Yang, *Phys. Rev.* **105**, 767 (1957).
- [59] K. Huang, C. N. Yang, and J. M. Luttinger, *Phys. Rev.* **105**, 776 (1957).
- [60] R. Dashen, S.-K. Ma, and H. J. Bernstein, *Phys. Rev.* **187**, 345 (1969).
- [61] R. Dashen and R. Rajaraman, *Phys. Rev. D* **10**, 708 (1974).

- [62] R. P. Feynman, *Photon-Hadron Interactions* (CRC Press, 2018).
- [63] B. Ioffe, *Phys. Lett. B* **30**, 123 (1969).
- [64] Y. V. Kovchegov and M. Strikman, *Phys. Lett. B* **516**, 314 (2001).
- [65] E. P. Wigner, *Phys. Rev.* **98**, 145 (1955).
- [66] M. Luscher, *Commun. Math. Phys.* **105**, 153 (1986).
- [67] M. Luscher, *Nucl. Phys. B* **354**, 531 (1991).
- [68] M. T. Hansen and S. R. Sharpe, *Annu. Rev. Nucl. Part. Sci.* **69**, 65 (2019).
- [69] R. A. Briceño, J. J. Dudek, and R. D. Young, *Rev. Mod. Phys.* **90**, 025001 (2018).
- [70] R. A. Briceño, J. V. Guerrero, M. T. Hansen, and A. Sturzu, *Phys. Rev. D* **103**, 014506 (2021).
- [71] S. J. Brodsky, H.-C. Pauli, and S. S. Pinsky, *Phys. Rep.* **301**, 299 (1998).
- [72] L. Susskind, *Phys. Rev.* **165**, 1535 (1968).
- [73] J. Bjorken, J. B. Kogut, and D. E. Soper, *Phys. Rev. D* **3**, 1382 (1971).
- [74] S. Weinberg, *Phys. Rev. Lett.* **18**, 188 (1967).
- [75] A. L. Fitzpatrick, E. Katz, and M. T. Walters, *J. High Energy Phys.* **10** (2020) 092.
- [76] N. Anand, A. L. Fitzpatrick, E. Katz, Z. U. Khandker, M. T. Walters, and Y. Xin, [arXiv:2005.13544](https://arxiv.org/abs/2005.13544) [hep-th] (2020).
- [77] J. Liu and Y. Xin, *J. High Energy Phys.* **12** (2020) 011.
- [78] A. J. A. James, R. M. Konik, P. Lecheminant, N. J. Robinson, and A. M. Tsvelik, *Prog. Part. Nucl. Phys.* **81**, 046002 (2018).
- [79] M. Kreshchuk, W. M. Kirby, G. Goldstein, H. Beauchemin, and P. J. Love, [arXiv:2002.04016](https://arxiv.org/abs/2002.04016) [quant-ph](2020).
- [80] M. Kreshchuk, S. Jia, W. M. Kirby, G. Goldstein, J. P. Vary, and P. J. Love, [arXiv:2009.07885](https://arxiv.org/abs/2009.07885) [quant-ph](2020).
- [81] C. W. Bauer, S. Fleming, D. Pirjol, and I. W. Stewart, *Phys. Rev. D* **63**, 114020 (2001).
- [82] F. Gelis, E. Iancu, J. Jalilian-Marian, and R. Venugopalan, *Annu. Rev. Nucl. Part. Sci.* **60**, 463 (2010).
- [83] E. Braaten and R. D. Pisarski, *Nucl. Phys. B* **337**, 569 (1990).
- [84] N. Klco and M. J. Savage, *Phys. Rev. A* **99**, 052335 (2019).
- [85] A. M. Childs, R. Kothari, and R. D. Somma, *SIAM J. Comput.* **46**, 1920 (2017).
- [86] A. Gilyén, Y. Su, G. H. Low, and N. Wiebe, in *Proceedings of the 51st Annual ACM SIGACT Symposium on Theory of Computing* (Association for Computing Machinery, New York, 2019), pp. 193–204.
- [87] H. F. Trotter, *Proc. Am. Math. Soc.* **10**, 545 (1959).
- [88] M. Suzuki, *Commun. Math. Phys.* **51**, 183 (1976).
- [89] C. Gerry and P. Knight, *Introductory Quantum Optics* (Cambridge University Press, Cambridge, 2004).
- [90] K. Yeter-Aydeniz and G. Siopsis, *Phys. Rev. D* **97**, 036004 (2018).
- [91] M. A. Nielsen and I. L. Chuang, *Quantum Computation and Quantum Information* (Cambridge University Press, 2010).
- [92] Q. Su, B. A. Smetanko, and B. Grobe, *Opt. Express* **2**, 277 (1997).
- [93] H. Lamm and S. Lawrence, *Phys. Rev. Lett.* **121**, 170501 (2018).
- [94] C. Kokail, C. Maier, R. van Bijnen, T. Brydges, M. K. Joshi, P. Jurcevic, C. A. Muschik, P. Silvi, R. Blatt, C. F. Roos *et al.*, *Nature (London)* **569**, 355 (2019).
- [95] A. Bapat and S. Jordan, *Quantum Inf. Comput.* **19**, 424 (2019).
- [96] S. Harmalkar, H. Lamm, and S. Lawrence, [arXiv:2001.11490](https://arxiv.org/abs/2001.11490) (2020).
- [97] E. J. Gustafson and H. Lamm, *Phys. Rev. D* **103**, 054507 (2020).
- [98] K. Choi and D. Lee, [arXiv:2009.04092](https://arxiv.org/abs/2009.04092) (2020).
- [99] G. Brassard, P. Hoyer, M. Mosca, and A. Tapp, *Contemp. Math.* **305**, 53 (2002).
- [100] D. W. Berry, A. M. Childs, R. Cleve, R. Kothari, and R. D. Somma, in *Proceedings of the 46th Annual ACM Symposium on Theory of Computing—STOC 14* (Association for Computing Machinery, New York, 2014).
- [101] L. Grover and T. Rudolph, [arXiv:quant-ph/0208112](https://arxiv.org/abs/quant-ph/0208112) (2002).
- [102] P. Kaye and M. Mosca, [arXiv:quant-ph/0407102](https://arxiv.org/abs/quant-ph/0407102) (2004).
- [103] A. Tranter, P. J. Love, F. Mintert, and P. V. Coveney, *J. Chem. Theory Comput.* **14**, 5617 (2018).
- [104] A. Kitaev and W. A. Webb, [arXiv:0801.0342](https://arxiv.org/abs/0801.0342) (2008).
- [105] V. Vedral, A. Barenco, and A. Ekert, *Phys. Rev. A* **54**, 147 (1996).
- [106] T. G. Draper, [arXiv:quant-ph/0008033](https://arxiv.org/abs/quant-ph/0008033) (2000).
- [107] Y. Cao, A. Papageorgiou, I. Petras, J. Traub, and S. Kais, *New J. Phys.* **15**, 013021 (2013).
- [108] E. Muoz-Coreas and H. Thapliyal, [arXiv:1712.08254](https://arxiv.org/abs/1712.08254) [quant-ph] (2018).
- [109] M. K. Bhaskar, S. Hadfield, A. Papageorgiou, and I. Petras, *Quantum Inf. Comput.* **16**, 0197 (2016).
- [110] T. Häner, M. Roetteler, and K. Svore, [arXiv:1805.12445](https://arxiv.org/abs/1805.12445) (2018).
- [111] C. Zalka, *Proc. R. Soc. London A* **454**, 313 (1998).
- [112] M. M. Nieto and D. R. Truax, *Fortschr. Phys.* **45**, 145 (1997).
- [113] K. Marshall, R. Pooser, G. Siopsis, and C. Weedbrook, *Phys. Rev. A* **92**, 063825 (2015).
- [114] A. F. Shaw, P. Lougovski, J. R. Stryker, and N. Wiebe, *Quantum* **4**, 306 (2020).
- [115] T. A. Brun, [arXiv:1910.03672](https://arxiv.org/abs/1910.03672) [quant-ph] (2019).
- [116] J. R. Stryker, *Phys. Rev. A* **99**, 042301 (2019).
- [117] M. C. Tran, Y. Su, D. Carney, and J. M. Taylor, *PRX Quantum* **2**, 010323 (2021).
- [118] H. Lamm, S. Lawrence, and Y. Yamauchi, [arXiv:2005.12688](https://arxiv.org/abs/2005.12688) (2020).
- [119] J. C. Halimeh, H. Lang, J. Mildenerger, Z. Jiang, and P. Hauke, [arXiv:2007.00668](https://arxiv.org/abs/2007.00668) (2020).
- [120] M. C. Tran, S.-K. Chu, Y. Su, A. M. Childs, and A. V. Gorshkov, *Phys. Rev. Lett.* **124**, 220502 (2020).
- [121] S. A. Cuccaro, T. G. Draper, S. A. Kutin, and D. P. Moulton, [arXiv:quant-ph/0410184](https://arxiv.org/abs/quant-ph/0410184) (2004).
- [122] D. S. Oliveira and R. V. Ramos, *Quantum Comput. Comput.* **7**, 17 (2007).
- [123] H. Xia, H. Li, H. Zhang, Y. Liang, and J. Xin, *Int. J. Theor. Phys.* **57**, 3727 (2018).
- [124] G. G. Guerreschi, *Phys. Rev. A* **99**, 022306 (2019).
- [125] A. Paetznick and K. M. Svore, *Quantum Inf. Comput.* **14**, 1277 (2014).
- [126] A. H. Mueller, *Phys. Lett. B* **104**, 161 (1981).
- [127] Y. Dokshitzer, *Basics of Perturbative QCD* (Atlantica Séguier Frontières, 1991).
- [128] B. Webber, *J. Mod. Phys. A* **15**, 577 (2000).
- [129] B. Andersson, *The Lund Model*, Cambridge Monographs on Particle Physics, Nuclear Physics and Cosmology (Cambridge University Press, Cambridge, 1998).

- [130] R. Cleve, A. Ekert, C. Macchiavello, and M. Mosca, *Proc. R. Soc. London A* **454**, 339 (1998).
- [131] D. S. Abrams and S. Lloyd, *Phys. Rev. Lett.* **83**, 5162 (1999).
- [132] E. Knill, G. Ortiz, and R. D. Somma, *Phys. Rev. A* **75**, 012328 (2007).
- [133] A. Roggero and A. Baroni, *Phys. Rev. A* **101**, 022328 (2020).
- [134] N. Mueller and R. Venugopalan, *Phys. Rev. D* **99**, 056003 (2019).
- [135] C. Robin, M. J. Savage, and N. Pillet, *Phys. Rev. C* **103**, 034325 (2021).
- [136] D. E. Kharzeev and E. M. Levin, *Phys. Rev. D* **95**, 114008 (2017).
- [137] Y. Hagiwara, Y. Hatta, B.-W. Xiao, and F. Yuan, *Phys. Rev. D* **97**, 094029 (2018).
- [138] A. Kovner, M. Lublinsky, and M. Serino, *Phys. Lett. B* **792**, 4 (2019).
- [139] Z. Tu, D. E. Kharzeev, and T. Ullrich, *Phys. Rev. Lett.* **124**, 062001 (2020).
- [140] J. Berges, S. Floerchinger, and R. Venugopalan, *Phys. Lett. B* **778**, 442 (2018).
- [141] J. Berges, S. Floerchinger, and R. Venugopalan, *J. High Energy Phys.* **04** (2018) 145.
- [142] B. Nachman, D. Provasoli, W. A. De Jong, and C. W. Bauer, *Phys. Rev. Lett.* **126**, 062001 (2021).
- [143] S. R. Beane and P. J. Ehlers, *Mod. Phys. Lett. A* **35**, 2050048 (2020).
- [144] A. Tarasov and R. Venugopalan, *Phys. Rev. D* **102**, 114022 (2020).
- [145] F. Wegner, *Ann. Phys.* **506**, 77 (1994).
- [146] R. J. Perry and K. G. Wilson, *Nucl. Phys. B* **403**, 587 (1993).
- [147] S. D. Glazek and K. G. Wilson, *Phys. Rev. D* **48**, 5863 (1993).
- [148] R. J. Perry, *Ann. Phys.* **232**, 116 (1994).
- [149] S. R. Beane and R. C. Farrell, [arXiv:2011.01278](https://arxiv.org/abs/2011.01278) [hep-th] (2020).
- [150] S. Bravyi, D. P. DiVincenzo, and D. Loss, *Ann. Phys.* **326**, 2793 (2011).
- [151] J. Otterbach, R. Manenti, N. Alidoust, A. Bestwick, M. Block, B. Bloom, S. Caldwell, N. Didier, E. S. Fried, S. Hong *et al.*, [arXiv:1712.05771](https://arxiv.org/abs/1712.05771) (2017).
- [152] A. Peruzzo, J. McClean, P. Shadbolt, M.-H. Yung, X.-Q. Zhou, P. J. Love, A. Aspuru-Guzik, and J. L. O'Brien, *Nat. Commun.* **5**, 4213 (2014).
- [153] A. Y. Kitaev, [arXiv:quant-ph/9511026](https://arxiv.org/abs/quant-ph/9511026) (1995).
- [154] E. Farhi, J. Goldstone, S. Gutmann, and M. Sipser, [arXiv:quant-ph/0001106](https://arxiv.org/abs/quant-ph/0001106) (2000).
- [155] E. Farhi, J. Goldstone, and S. Gutmann, [arXiv:1411.4028](https://arxiv.org/abs/1411.4028) (2014).
- [156] M. Motta, C. Sun, A. T. Tan, M. J. O'Rourke, E. Ye, A. J. Minnich, F. G. Brandão, and G. K.-L. Chan, *Nat. Phys.* **16**, 205 (2020).
- [157] M. T. Hansen, H. B. Meyer, and D. Robaina, *Phys. Rev. D* **96**, 094513 (2017).
- [158] S. M. Girvin, *Quantum Machines* **113**, 2 (2011).
- [159] A. M. Childs, Y. Su, M. C. Tran, N. Wiebe, and S. Zhu, *Phys. Rev. X* **11**, 011020 (2021).
- [160] A. Steane, *Proc. R. Soc. London A* **452**, 2551 (1996).
- [161] A. M. Steane, in *Proceedings of the International School of Physics Enrico Fermi*, Vol. 162 (IOS Press, Amsterdam, 2007), p. 1.
- [162] A. R. Calderbank and P. W. Shor, *Phys. Rev. A* **54**, 1098 (1996).
- [163] A. Macridin, P. Spentzouris, J. Amundson, and R. Harnik, *Phys. Rev. Lett.* **121**, 110504 (2018).
- [164] A. Macridin, P. Spentzouris, J. Amundson, and R. Harnik, *Phys. Rev. A* **98**, 042312 (2018).
- [165] R. Brower, S. Chandrasekharan, and U.-J. Wiese, *Phys. Rev. D* **60**, 094502 (1999).
- [166] D. Banerjee, M. Bögli, M. Dalmonte, E. Rico, P. Stebler, U.-J. Wiese, and P. Zoller, *Phys. Rev. Lett.* **110**, 125303 (2013).
- [167] E. Zohar, J. I. Cirac, and B. Reznik, *Rep. Prog. Phys.* **79**, 014401 (2015).
- [168] N. Klco, M. J. Savage, and J. R. Stryker, *Phys. Rev. D* **101**, 074512 (2020).
- [169] V. Kasper, G. Juzeliunas, M. Lewenstein, F. Jendrzejewski, and E. Zohar, *New J. Phys.* **22**, 103027 (2020).
- [170] Z. Davoudi, I. Raychowdhury, and A. Shaw, [arXiv:2009.11802](https://arxiv.org/abs/2009.11802) [hep-lat] (2020).
- [171] R. Dasgupta and I. Raychowdhury, [arXiv:2009.13969](https://arxiv.org/abs/2009.13969) (2020).
- [172] A. Accardi, J. Albacete, M. Anselmino, N. Armesto, E. Aschenauer, A. Bacchetta, D. Boer, W. Brooks, T. Burton, N.-B. Chang *et al.*, *Eur. Phys. J. A* **52**, 268 (2016).
- [173] D.-B. Zhang, H. Xing, H. Yan, E. Wang, and S.-L. Zhu, *Chin. Phys. B* **30**, 020306 (2021).
- [174] A. Krasnitz and R. Venugopalan, *Nucl. Phys. B* **557**, 237 (1999).
- [175] J. Berges, S. Schlichting, and D. Sexty, *Phys. Rev. D* **86**, 074006 (2012).
- [176] M. Mace, N. Mueller, S. Schlichting, and S. Sharma, *Phys. Rev. Lett.* **124**, 191604 (2020).
- [177] Q. A. Turchette, C. J. Hood, W. Lange, H. Mabuchi, and H. J. Kimble, *Phys. Rev. Lett.* **75**, 4710 (1995).
- [178] P. Kaye, [arXiv:quant-ph/0407095](https://arxiv.org/abs/quant-ph/0407095) (2005).
- [179] P. Kaye, [arXiv:quant-ph/0408173](https://arxiv.org/abs/quant-ph/0408173) (2004).
- [180] V. Zakharov, V. Lvov, and G. Falkovich, *Kolmogorov Spectra of Turbulence I: Wave Turbulence* (Springer Verlag, 1992).
- [181] J. Deng, S. Schlichting, R. Venugopalan, and Q. Wang, *Phys. Rev. A* **97**, 053606 (2018).
- [182] S. Bogner, R. Furnstahl, and A. Schwenk, *Prog. Part. Nucl. Phys.* **65**, 94 (2010).